Journal of Hydrology 414–415 (2012) 1–15

Contents lists available at SciVerse ScienceDirect

Journal of Hydrology

journal homepage: www.elsevier.com/locate/jhydrol

Wet canopy evaporation from a Puerto Rican lower montane rain forest: The importance of realistically estimated aerodynamic conductance

F. Holwerda [a,b,*], L.A. Bruijnzeel [a], F.N. Scatena [c], H.F. Vugts [a], A.G.C.A. Meesters [a]

[a] Department of Hydrology and Geo-Environmental Sciences, Faculty of Earth and Life Sciences, VU University, Amsterdam, The Netherlands
[b] Centro de Ciencias de la Atmósfera, Universidad Nacional Autónoma de México, Ciudad de México, DF, Mexico
[c] Department of Earth and Environmental Science, University of Pennsylvania, Philadelphia, PA, USA

ARTICLE INFO

Article history:
Received 5 April 2011
Received in revised form 6 July 2011
Accepted 23 July 2011
Available online 29 July 2011

This manuscript was handled by Konstantine P. Georgakakos, Editor-in-Chief, with the assistance of Christa D. Peters-Lidard, Associate Editor

Keywords:
Aerodynamic conductance
Evaporation
Interception
Sensible heat flux
Throughfall
Topography

SUMMARY

Rainfall interception (I) was measured in 20 m tall Puerto Rican tropical forest with complex topography for a 1-year period using totalizing throughfall (TF) and stemflow (SF) gauges that were measured every 2–3 days. Measured values were then compared to evaporation under saturated canopy conditions (E) determined with the Penman–Monteith (P–M) equation, using (i) measured (eddy covariance) and (ii) calculated (as a function of forest height and wind speed) values for the aerodynamic conductance to momentum flux ($g_{a,M}$). E was also derived using the energy balance equation and the sensible heat flux measured by a sonic anemometer (H_s). I per sampling occasion was strongly correlated with rainfall (P): $I = 0.21P + 0.60$ (mm), $r^2 = 0.82$, $n = 121$. Values for canopy storage capacity ($S = 0.37$ mm) and the average relative evaporation rate ($E/R = 0.20$) were derived from data for single events ($n = 51$). Application of the Gash analytical interception model to 70 multiple-storm sampling events using the above values for S and E/R gave excellent agreement with measured I. For $E/R = 0.20$ and an average rainfall intensity (R) of 3.16 mm h^{-1}, the TF-based E was 0.63 mm h^{-1}, about four times the value derived with the P–M equation using a conventionally calculated $g_{a,M}$ (0.16 mm h^{-1}). Estimating $g_{a,M}$ using wind data from a nearby but more exposed site yielded a value of E (0.40 mm h^{-1}) that was much closer to the observed rate, whereas E derived using the energy balance equation and H_s was very low (0.13 mm h^{-1}), presumably because H_s was underestimated due to the use of too short a flux-averaging period (5-min). The best agreement with the observed E was obtained when using the measured $g_{a,M}$ in the P–M equation (0.58 mm h^{-1}). The present results show that in areas with complex topography, $g_{a,M}$, and consequently E, can be strongly underestimated when calculated using equations that were derived originally for use in flat terrain; hence, direct measurement of $g_{a,M}$ using eddy covariance is recommended. The currently measured $g_{a,M}$ (0.31 m s^{-1}) was at least several times, and up to one order of magnitude higher than values reported for forests in areas with flat or gentle topography (0.03–0.08 m s^{-1}, at wind speeds of about 1 m s^{-1}). The importance of $g_{a,M}$ at the study site suggests a negative, downward, sensible heat flux sustains the observed high evaporation rates during rainfall. More work is needed to better quantify H_s during rainfall in tropical forests with complex topography.

© 2011 Elsevier B.V. All rights reserved.

1. Introduction

Based on a preliminary comparison of the high rainfall interception losses reported for a temperate forest (Wales, UK) subjected to oceanic influences, with the much lower losses from a tropical rain forest situated in the middle of a continent (Manaus, Brazil), Shuttleworth (1989) hypothesized that tropical deforestation at continental-edge and island locations was likely to have a greater effect on streamflow than would deforestation at mid-continental sites. Since then, a substantial number of interception studies conducted in tropical forests subject to 'maritime' climatic conditions have yielded interception values that were generally much higher (at 18–50% of incident rainfall; summarized by Schellekens et al. (2000), Roberts et al. (2005), and Wallace and McJannet (2008)) than those typically observed at mid-continental locations (9–17%; see discussion in Roberts et al., 2005; cf. Cuartas et al., 2007). Similarly, average wet-canopy evaporation rates (E) inferred from throughfall (TF) measurements under maritime tropical conditions (0.4–1.0 mm h^{-1}) are typically 4–5 times those calculated with the Penman–Monteith (P–M) equation (Schellekens et al., 1999; Roberts et al., 2005; Wallace and McJannet, 2008). No such discrepancy appears to have been encountered under continental tropical conditions (Lloyd et al., 1988; Cuartas et al., 2007).

* Corresponding author. Address: Centro de Ciencias de la Atmósfera, Universidad Nacional Autónoma de México, Circuito exterior s/n, Cd. Universitaria, 04510 Coyoacán, Ciudad de México, DF, Mexico.

E-mail address: friso.holwerda@gmail.com (F. Holwerda).

0022-1694/$ - see front matter © 2011 Elsevier B.V. All rights reserved.
doi:10.1016/j.jhydrol.2011.07.033

Several possible reasons for the high interception losses and for the discrepancy between *TF*-based and P–M-based rates of *E* under maritime tropical conditions have been suggested in the literature, including:

(i) underestimation of *TF* due to inadequate sampling design (Dykes, 1997; Schellekens et al., 1999, 2000; cf. Lloyd and Marques, 1988; Ziegler et al., 2009; Zimmermann et al., 2010);
(ii) advection of sensible heat from the nearby ocean (Dykes, 1997; Waterloo et al., 1999; Schellekens et al., 1999, 2000; Wallace and McJannet, 2008; cf. Shuttleworth and Calder, 1979; Shuttleworth, 1989; Roberts et al., 2005); and
(iii) underestimation of the aerodynamic conductance (Schellekens et al., 1999, 2000; cf. Gash et al., 1980).

Holwerda et al. (2006) investigated the influence of underestimated *TF* by quantifying the variability of *TF* and the standard errors of the means associated with the deployment of 60 fixed, 30 fixed, and 30 roving gauges in the same Puerto Rican forest for which Scatena (1990) and Schellekens et al. (1999, 2000) had previously obtained very high interception losses. Holwerda et al. (2006) reported total *TF* values as measured with the fixed and roving sampling designs to be nearly equal, although the variability of the estimate was about half as high in the case of roving gauges. Furthermore, the sampling methods used by several *TF* studies reporting high interception losses under maritime tropical conditions, e.g. Dykes (1997) (17 roving gauges with 314 cm^2 orifice each), Waterloo et al. (1999) (20 roving gauges, 100 cm^2 orifice each), and Wallace and McJannet (2008) (4–6 large troughs with dynamically calibrated tipping buckets) all seem to have been adequate. As such, there is no reason to believe that an underestimation of *TF* caused the high interception losses observed at these maritime sites.

Roberts et al. (2005) discussed the role of advected energy and estimated that for an advection-driven evaporation rate of 100 $W\,m^{-2}$ (equivalent to $\sim$0.15 $mm\,h^{-1}$), a horizontal temperature gradient of 1 K per 100 m would be required. Hence, to explain a typically observed difference of 0.5 $mm\,h^{-1}$ between *TF*-based and calculated (P–M-based) rates of *E* for maritime tropical sites (see Table 4 below), a (persistent) horizontal temperature gradient of 3–4 K per 100 m would be necessary. This is considered unrealistic given the average distance from the coast of these sites is approximately 17 km.

The alternative explanation for greatly enhanced *E*, i.e. underestimation of the aerodynamic conductance for momentum transfer ($g_{a,M}$), has received comparatively little attention under tropical and temperate conditions alike (e.g. Gash et al., 1980; Schellekens et al., 1999, 2000). With very few exceptions (e.g. Gash et al., 1999; Van der Tol et al., 2003; Cuartas et al., 2007; Herbst et al., 2008), rainfall interception modeling studies have typically estimated *E* with the P–M equation using the equation for momentum transfer of Thom (1975) to calculate $g_{a,M}$ (see Muzylo et al. (2009) for an overview of interception modeling studies world-wide). However, strictly speaking, the Thom equation is valid over uniform, extensive, and flat surfaces only (Monteith and Unsworth, 2008) and its application to forests located in complex terrain, where patterns of wind flow and turbulence are affected by topography, is problematic (cf. Chen and Schwerdtfeger, 1989; Raupach and Finnigan, 1997; see also Section 2).

This paper investigates whether underestimation of $g_{a,M}$ through the conventional use of the Thom formula can explain the major discrepancy between observed (*TF*-based) and calculated rates of wet-canopy evaporation for the Puerto Rican lower montane rain forest studied previously by Scatena (1990) and Schellekens et al. (1999). Micrometeorological and net precipitation data were collected between November 2000 and October 2001. *E* rates were calculated using the P–M equation with $g_{a,M}$ either estimated from the Thom equation or measured directly by the eddy covariance method (see Section 2). Wet canopy evaporation was also calculated using the energy balance equation and the sensible heat flux as measured by a sonic anemometer (see Section 2). The evaporation rates obtained by the respective methods are then compared with values inferred from the rainfall, throughfall, and stemflow measurements.

2. Theory

The evaporation from a wet canopy is conventionally calculated using the Penman–Monteith equation (Monteith, 1965):

$$\lambda E = \frac{\Delta A + \rho c_p VPD g_a}{\Delta + \gamma} \tag{1}$$

in which Δ is the slope of the saturated vapor pressure–temperature relationship at temperature T (kPa K^{-1}), A the available energy (W m^{-2}) (in this study assumed to be equal to the net radiation R_n), ρ the density of air (kg m^{-3}), c_p the specific heat of air at constant pressure (J kg^{-1} K^{-1}), *VPD* the vapor pressure deficit (kPa), γ the psychrometric constant (kPa K^{-1}), g_a the aerodynamic conductance (m s^{-1}), and λ the latent heat of vaporization of water (J kg^{-1}).

The aerodynamic conductance (g_a) is usually estimated with the equation for momentum transfer of Thom (1975), with an added term to correct for non-neutral atmospheric stability conditions (Paulson, 1970; Webb, 1970; Monteith and Unsworth, 2008):

$$g_{a,M} = \left\{\frac{k}{\ln[(z-d)/z_{0,M}] - \psi_M}\right\}^2 u \tag{2}$$

in which k is von Karman's constant (0.41), d the zero-plane displacement (m), $z_{0,M}$ the roughness length for momentum (m), u (m s^{-1}) the wind speed measured at height z (m), and ψ_M is an integrated stability correction function. Atmospheric stability is evaluated as $(z-d)/L$, where L is the Monin–Obukhov length (see Section 3; Monteith and Unsworth, 2008).

The aerodynamic conductance may also be derived in a more direct manner using the friction velocity (u_*, m s^{-1}) as obtained from sonic anemometer measurements (Gash et al., 1999; Van der Tol et al., 2003):

$$g_{a,M} = \left(\frac{u_*}{u}\right)^2 u \tag{3}$$

The friction velocity (u_*) is given by (Stull, 1988; Weber, 1999):

$$u_* = \left(\overline{u'w'}^2 + \overline{v'w'}^2\right)^{0.25} \tag{4}$$

where $\overline{u'w'}$ and $\overline{v'w'}$ are the co-variances of the turbulent fluctuations of the horizontal (u', v') and vertical (w') wind components as measured with a sonic anemometer.

It is pertinent to note that Eq. (2) is based on the Monin–Obukhov similarity theory, which only holds under conditions of an extended, uniform, and flat surface (e.g. Monteith and Unsworth, 2008). In addition, similarity theory is only valid for the inertial sub-layer of the atmospheric boundary layer, whilst closer to the surface (i.e. in the roughness and transitional sub-layers) 'similarity breakdown' occurs (e.g. Thom et al., 1975; Simpson et al., 1998). As discussed by Chen and Schwerdtfeger (1989), the sub-layer with similarity breakdown tends to become more extended as the topographic complexity of the terrain is more pronounced. In such environments, u_* is enhanced (compared to 'uniform' environments experiencing the same large-scale flow), whereas at the same time u at the measurement level tends to decrease. The latter is related to the increase of the average du/dz above the measurement level, where du/dz scales with the increased u_*. The decrease in u is reflected in the decreased ratio of du/dz to u_* at the measurement level, and is always observed as the forest surface becomes less uniform (see survey by Chen and Schwerdtfeger (1989)). As a result, according to Eq. (3), $g_{a,M}$ in a complex environment will be enhanced relative to a uniform environment. Under such conditions, the conventional application of Eq. (2), with $g_{a,M}$ estimated from canopy properties, will yield a value that is often much too low.

Another problem with the application of Eq. (2) relates to the fact that the process of momentum transfer through the turbulent boundary layer differs from the transfer of scalars like water vapor or sensible heat (Thom, 1972). The roughness length for momentum ($z_{0,M}$) is much greater than that for heat and vapor ($z_{0,H}$) (Garratt and Francey, 1978). However, the use of $g_{a,M}$ in the calculation of wet-canopy evaporation with the Penman–Monteith equation has generally given good results (Rutter et al., 1975; Shuttleworth, 1989; cf. Gash et al., 1999). The reason for this apparent contradiction is again the distortion of similarity theory, this time for scalar transport, within the roughness sub-layer (see Shuttleworth (1989) for further explanation; cf. Simpson et al., 1998).

E can also be derived using the energy balance equation and the sensible heat flux measured by a sonic anemometer (Van der Tol et al., 2003; cf. Mizutani et al., 1997):

$$\lambda E = \frac{A - H_s - C_2 - J}{1 - C_1} \tag{5}$$

where H_s is the sensible heat flux derived from the fluctuations of w and the temperature (T_s) measured by a sonic anemometer:

$$H_s = \rho c_p \overline{w'T'_s} \tag{6}$$

and J is the change in storage of sensible and latent heat below the measurement level (see Section 3).

The terms C_1 and C_2 come from the equation that relates H_s to the 'true' sensible heat flux and are calculated as (Liu et al., 2001):

$$C_1 = 0.51 \frac{c_p}{\lambda} T \tag{7}$$

$$C_2 = \frac{3T\rho c_p}{2c^2} \left(\overline{w'u'}u + \overline{w'v'}v \right) \tag{8}$$

where T is the average air temperature (K) and c the speed of sound (m s^{-1}).

Although the derivation of E using Eq. (5) and H_s is the most direct way to estimate wet-canopy evaporation, the determination of H_s in complex terrain and under rainy conditions is not without problems. The use of the eddy covariance technique depends on several assumptions, the most important of which are stationarity and homogeneity of the flow field, i.e. the statistical properties of the flow must be constant in time and space, respectively (e.g. Foken and Wichura, 1996). However, in mountainous terrain, both wind and temperature fields are strongly influenced by the topography (Raupach and Finnigan, 1997) so that the assumption of homogeneity is usually not met (cf. Bernhofer, 1992). Further, the evaporation of intercepted rainfall is usually maintained by a negative (downward) sensible heat flux (e.g. Mizutani et al., 1997). If wind speeds are low, a negative sensible heat flux implies stable atmospheric conditions, and hence, suppressed turbulence. Under such conditions, the turbulence is often intermittent and non-stationary, and the value of H_s derived with Eq. (6) depends strongly on the flux-averaging period used (Acevedo et al., 2006).

3. Materials and methods

3.1. Site characteristics

The present study was conducted in the 6.4 ha Bisley 2 catchment, which is located at 18°19′N and 65°44′W at elevations between 265 and 456 m a.s.l. in the Luquillo Mountains, northeastern Puerto Rico (Fig. 1). The catchment is covered with Tabonuco-type rain forest, with an average canopy height (h_c, m) of about 20 m (Scatena and Lugo, 1995; Schellekens et al., 2000). The understorey consists mainly of palms and ground-level herbs and shrubs (Scatena and Lugo, 1995). The Bisley forest is regularly hit by hurricanes, with the last event that caused considerable damage to the forest being hurricane Hugo in 1989 (Scatena and Lugo, 1995). Smaller damage was caused subsequently by hurricanes Bertha and Hortense in 1996 and by Georges in 1998. However, the forest canopy generally recovers rapidly from hurricane-related damage (Scatena et al., 1996). At the time of the present study (2000/2001), the leaf area index (LAI, m^2 m^{-2}) of the forest (6.7; Holwerda, 2005) was again very similar to the pre-Hugo value of 6.4 (Odum et al., 1970).

The terrain is steep and dissected; slopes in excess of 45% (24°) cover more than 50% of the catchment (Schellekens et al., 2000), which runs from the southeast towards the northwest (Fig. 1). The micrometeorological measurements were made from a 24 m high scaffolding tower, located on the northeastern water divide at an elevation of about 335 m (henceforth referred to as the lower Bisley tower). The divide slopes towards the northwest at an average gradient of about 30% (17°). The slopes immediately to the north and south of the tower are oriented towards the north and west-southwest, respectively, with average gradients of about 50% (27°) and typical slopes lengths between 50 and 100 m.

A second 25 m high scaffolding tower (operated by the US Geological Survey) was located on the southwest to northeast oriented ridge that forms the southeastern water divide of the Bisley 2 catchment (ca. 400 m a.s.l., Fig. 1). This tower will be referred to as the upper Bisley tower. Because of its direct exposure to the easterly trade winds, the upper Bisley tower has a much longer fetch than the lower tower located on the lee-side of the ridge (Fig. 1; see also Section 4).

The climate is maritime tropical, type A2m according to the Köppen classification. Annual rainfall is about 3500 mm, and distributed fairly evenly throughout the year; in general, May and November are the wettest months with about 385 mm each, whilst the January–March period is relatively 'dry' with about 200 mm per month on average (García-Martinó et al., 1996; Heartsill-Scalley et al., 2007). Although rain is more common at night than during the day, the diurnal distribution of rainfall is very even, indicating that rainfall intensities are lower on average at night than during the day (Schellekens et al., 2000; see also Section 4). Mean monthly temperatures vary little (24 °C in winter versus 27–28 °C in summer), and seasonal variation in average daily relative humidity is small (84–90%; Brown et al., 1983). The wind regime at Bisley is characterized by northerly (anabatic, upslope) and southerly (katabatic, downslope) winds during the day and night, respectively, with an average speed of 1–2 m s^{-1} (Van der Molen, 2002). Because Bisley is situated only 10 km from the Atlantic coast, it is also influenced by the (northerly) sea breeze (Van der Molen, 2002). At exposed sites, such as the location of the upper tower (Fig. 1), wind speeds are stronger (about 4 m s^{-1}) and from a more constant (easterly) direction (see Section 4).

3.2. Measurements

3.2.1. Rainfall, throughfall, and stemflow

Rainfall (P, mm) was measured with an ARG100 (Environmental Measurements Ltd.; 0.20 mm resolution) tipping bucket rain gauge, installed on the 24 m lower Bisley tower. The rain gauge was connected to a Campbell Scientific Ltd. 21X data-logger and 5-min totals were stored in an external storage module. The readings by the ARG100 (x) were within 1% of those by a Casella CEL tipping bucket rain gauge ($y = 0.99x + 0.05$ (mm h^{-1}), $r^2 = 0.96$)

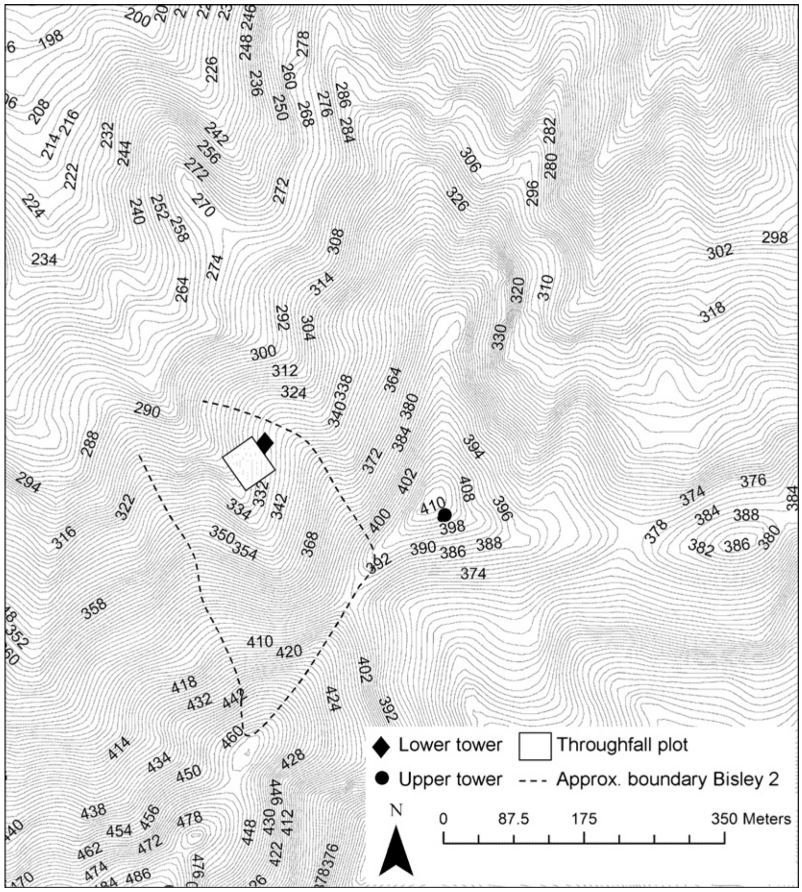

Fig. 1. Topography of the Bisley 2 catchment (north-eastern Puerto Rico) and surroundings. Elevations are in meters and contour line spacing is 2 m.

and a totalizing gauge ($y = 0.99x + 0.30$ (mm per sampling occasion), $r^2 = 0.99$) that were located on the same tower (the totalizer gauge was read at the same time as the throughfall measurements, i.e. approximately every 2–3 days).

Throughfall (*TF*, mm) was measured on the northern slope of the catchment (directly to the south of the lower Bisley tower, Fig. 1) using three different gauge arrangements that were designed to test the influence of sampling design on *TF* estimates (Holwerda et al., 2006). The first arrangement was in use from November 2000 to March 2001 and consisted of 60 fixed gauges. The other two arrangements consisted of 30 fixed and 30 roving gauges, respectively. These two set-ups were run jointly between March and July 2001. From July until November 2001, measurements were made using the 30 roving gauges only. The latter were relocated to a new position each time the gauges were emptied, typically every 2–3 days. The gauges had a 100 cm^2 orifice positioned at about 30 cm above the ground and were kept level using steel holders. The funnels had 1.5 cm vertical risers to reduce splash losses. Further details are given by Holwerda et al. (2006).

Stemflow (*SF*, mm) was measured on 22 trees of four dominant species. The sampled tree species were *Dacryodes excelsa* (Tabonuco), *Prestoa montana* (a frequently occurring palm), *Sloanea berteriana*, and *Cecropia peltata*. At 1.0–1.5 m from the ground, PVC tubing slit open lengthwise was attached to the stem in a spiral fashion. Any remaining spaces between tubing and stem were sealed with silicon sealant. Areal *SF* was estimated by multiplying mean *SF* volume per tree species by the density of stems per hectare (>2.5 cm in diameter). An estimate of *SF* for other species, taken from Scatena (1990), was added to this value. Further details on *SF* measurements and up-scaling to the stand level can be found in Holwerda et al. (2006).

3.2.2. Micrometeorological measurements

Measurements of incoming and outgoing short- and long-wave radiation (W m^{-2}) were made at 24 m on the lower Bisley tower using a CM7 albedometer (Kipp and Zonen) and two precision infrared radiometers (The Eppley Laboratory). Net radiation (R_n, W m^{-2}) was calculated by adding the short- and long-wave radiation components. Temperature (T, °C) and relative humidity (*RH*, %) were measured at 4, 20, 24, and 27 m using combined *T*/*RH* sensors (HMP45, Vaisala). Actual vapor pressure (*VPA*, kPa) and vapor pressure deficit (*VPD*, kPa) were calculated from *RH* and the saturation vapor pressure (*SVP*, kPa) of the air at temperature *T*. *VPA* was also calculated from dry- (T_d) and wet-bulb (T_w) temperatures measured at 27 m using thermo-couples (VU University, Amsterdam). There was good agreement between values of *VPD* derived from the *T*/*RH* sensor at 27 m (y) and the thermo-couples (x) under wet canopy conditions (defined further below): $y = 0.95x + 0.02$ (kPa), $r^2 = 0.91$, $n = 507$ h), giving confidence in the humidity data. The values of *VPD* derived from the *T*/*RH* sensor were used in the present analysis. Wind speed (U, m s^{-1}) and wind direction (U_{dir}, degrees) were measured using an A100R cup anemometer and a W200P wind vane (Vector Instruments), respectively, both at 27 m. Note that in the present analysis the wind speed data from the sonic anemometer were used (see below). All of the above measurements were taken every 30 s by the 21X data-logger, and 5-min averages were stored in the external storage module.

Measurements of the horizontal (u, v, m s^{-1}) and vertical (w, m s^{-1}) wind components were made at 27 m using a Solent R3 sonic anemometer (Gill Instruments). The sonic anemometer also measured the sonic temperature (T_s). The anemometer was connected to a Campbell Scientific Ltd. 23X data-logger, which measured the signals every 0.1 s (10 Hz sampling rate). The data were stored in two different ways: (1) in a low data output (continuous) mode; and (2) in a high data output (intermittent) mode. In continuous mode, means, standard deviations, co-variances, and correlation coefficients were stored every 5-min in a low capacity data storage module, whereas in intermittent mode the raw (10 Hz) data were stored in a high capacity memory module. Note that the raw turbulence data were only stored for selected daytime periods during which the weather conditions were dry and predominantly sunny. For periods with rainfall, which are the focus of the present analysis, only the 5-min average fluxes as recorded by the data logger were available. As such, it was not possible to re-calculate the fluxes using a longer averaging time, which affected the results of this study considerably as will be shown below.

The raw u, v, w data were corrected for angle of attack errors resulting from the imperfect (co)sine response of the sonic anemometer (Gash and Dolman, 2003; Van der Molen et al., 2004), using the correction functions of Nakai et al. (2006). Next, two rotations were applied to the wind data to align: (i) u in the mean wind direction (i.e. $\bar{v} = 0$); and (ii) w normal to u (i.e. $\bar{w} = 0$) (Kaimal and Finnigan, 1994). The averaging time used was 5 min. The 5-min turbulence data stored by the data-logger in continuous mode ('data-logger data') were subjected to the same coordination rotation as the raw data, using the algorithms given by Sozzi and Favaron (1996). The data-logger data were corrected for angle of attack error by comparing them with the values derived from the raw data using linear regression.

3.2.3. Eddy covariance data quality assessment

Stationarity of the flow is usually evaluated by comparing the covariance calculated over the flux averaging period (e.g. 30-min) with the mean of the covariances calculated over shorter intervals (e.g. the mean of six 5-min covariances). The measurement is considered to be stationary when the difference between the covariances is less than 30% (Foken and Wichura, 1996). In the present study, turbulence data were stored as 5-min averages (continuous mode, see above) and it was not possible, therefore, to calculate covariances over different time intervals. Hence, stationarity was evaluated by comparing hourly means and standard deviations (SD) of the 5-min covariances; the measurement was considered to be stationary when SD was less than 30% of the mean.

The quality of the turbulence data was further evaluated by comparing the observed integral turbulence characteristics (ITC) of the vertical (σ_w/u_*) and horizontal (σ_u/u_*) wind components, and temperature (σ_{Ts}/T_*, $T_* = -\overline{w'T_s'}/u_*$) with the corresponding values predicted by similarity theory (Foken and Wichura, 1996). ITC are functions of atmospheric stability ($(z-d)/L$) and differences between measured and predicted values may indicate disturbance of the flow field by e.g. topography (Foken and Wichura, 1996). A threshold value of 30% for the percent difference between measured and predicted ITC is commonly used to separate high quality turbulence data from data reflecting disturbed conditions (Foken and Wichura, 1996). Theoretical values of the ITC were calculated following Thomas and Foken (2002).

The ITC test can also be used to evaluate the performance of the sonic anemometer during rainfall, i.e. if the effect of the rain would be to produce 'spikes' in the wind and temperature data recorded by the sonic anemometer, the values of the ITC during rainy conditions should be higher than those observed under dry conditions.

3.3. Rainfall interception loss

3.3.1. The Gash analytical interception model

Rainfall interception loss (I, mm) was determined as the difference between P and $TF + SF$. The interception data were analyzed using the Gash (1979) model (Table 1). The model uses event-based rainfall as input and assumes that the canopy dries up completely between events. Rainfall events were defined as periods with more than 0.2 mm of rain, separated by a dry period of at least 3 h (cf. Schellekens et al., 1999).

Table 1
The Gash (1979) interception model. See text for further explanation.

Component of interception loss	Formulation
For m storms too small to saturate the canopy ($P < P'$)	$(1-p-p_t)\sum_{j=1}^{m} P_j$
Wetting up the canopy for n storms large enough to saturate the canopy ($P \geqslant P'$)	$n(1-p-p_t)P' - nS$
Evaporation from the saturated canopy during rainfall	$\overline{E}/\overline{R}\sum_{j=1}^{n}(P_j - P')$
Evaporation after the rainfall event	nS
Evaporation from stems for q storms large enough to fill the trunk storage ($P \geqslant S_t/p_t$)	qS_t
Evaporation from stems for storms with $P < S_t/p_t$	$p_t\sum_{j=1}^{m+n-q} P_j$

The Gash model uses four canopy parameters (Table 1). The free TF coefficient (p) is the fraction of P that falls onto the ground without touching the vegetation. The parameter p_t is the fraction of P that is diverted to SF. The parameters S and S_t (both in mm) represent the amounts of water that can be stored on the canopy and stems, respectively.

The evaporation during rainfall is described by the relative evaporation rate ($\overline{E}/\overline{R}$), defined as the ratio of the mean wet-canopy evaporation rate ($\overline{E}$, mm h^{-1}) to mean rainfall rate ($\overline{R}$, mm h^{-1}); wet canopy conditions are assumed to occur when hourly $P > 0.50$ mm h^{-1} (Gash, 1979).

3.3.2. Derivation of the model parameters

The two SF-related parameters (p_t, S_t) were derived from the SF measurements (cf. Gash and Morton, 1978). The two canopy parameters (p, S) as well as the relative evaporation rate ($\overline{E}/\overline{R}$) were obtained using the 'mean method' of Klaassen et al. (1998). In this approach, p is determined from the linear relationship between P and I for storms smaller than the amount of rainfall required to saturate the canopy (P'):

$$I = a_1 P \tag{9a}$$

$$a_1 = (1 - p - p_t) \tag{9b}$$

whereas S and $\overline{E}/\overline{R}$ are derived from the I–P relationship for storms with $P \geqslant P'$:

$$I = a_2 P + b \tag{10a}$$

$$a_2 = \overline{E}/\overline{R} \tag{10b}$$

$$b = S \tag{10c}$$

First, a_1, a_2, and b are derived from Eqs. (9a) and (10a), using an estimate for P' based on the I–P graph. Next, P' is calculated as $P' = b/(a_1 - a_2)$, with the regression coefficients derived again using this new value of P'. This procedure is repeated until a continuous fit is obtained for Eqs. (9a) and (10a) at P' (Klaassen et al., 1998).

3.4. Wet-canopy evaporation

The average wet-canopy evaporation rate ($\overline{E}$) was derived from the value of $\overline{E}/\overline{R}$ as obtained from the interception data and from the average rainfall rate ($\overline{R}$) as measured by the tipping bucket rain gauge. The value of $\overline{E}$ derived in this way will be referred to in the following as the 'observed' or 'TF-based' evaporation rate.

E was also calculated using the Penman–Monteith equation (Eq. (1)), with $g_{a,M}$ determined in three different ways: (i) using Eq. (2) and wind data from the lower Bisley tower; (ii) idem with wind data from the upper, more exposed tower; and (iii) based on the friction velocity derived from eddy correlation measurements

(Eqs. (3) and (4)). In the former two cases, the values of d and z_0 were taken as $0.75h_c$ and $0.10h_c$, respectively (Shuttleworth, 1988). For z and h_c, the values for the lower Bisley tower site were used (27 m and 20 m, respectively). Wind data from the upper tower were obtained from the website of the US Geological Survey (US Geological Survey, 2010). The values of $g_{a,M}$ derived with Eq. (2) are referred to henceforth as the 'calculated' aerodynamic conductance, whereas those derived directly from the sonic anemometer measurements will be referred to as 'measured' aerodynamic conductance.

For non-neutral data, values of $g_{a,M}$ derived with Eq. (2) were corrected for the effects of atmospheric stability ($(z - d)/L$). The Monin–Obukhov length (L) was estimated as $-u_*^3/(k(g/T_s)\overline{w'T_s'})$, where g is the acceleration due to gravity (9.8 m s^{-2}) and the other terms are as defined previously (Monteith and Unsworth, 2008). Conditions during rain were mostly neutral or stable, so that the effect of the corrections was to reduce the value of $g_{a,M}$ somewhat (by −10% on average).

E was also calculated using the energy balance equation (Eq. (5)) and the sensible heat flux measured by the sonic anemometer (H_s, Eq. (6)). The change in storage of sensible and latent heat (J) was calculated from changes in temperature and humidity measured at the four levels (Thom, 1975). The value of E derived using Eqs. (5) and (6) will be referred to as the 'eddy covariance-based' evaporation rate.

4. Results

4.1. Rainfall

Between 1 November 2000 and 31 October 2001, a total of 2420 mm of rainfall (P) was measured, which was about 30% less than the long-term annual average of approximately 3500 mm (Heartsill-Scalley et al., 2007). Mean monthly P was 202 ± 68 (SD) mm, with minima of 110 and 123 mm in January and March, respectively, and maxima of 318 and 291 mm in August and October, respectively.

A total of 335 discrete rainfall events were identified from the hourly time series. The distribution of event size was positively skewed, as indicated by the difference between average (7.1 ± 15.0 mm) and median (2.8 mm) values (range: 0.4–176.9 mm). Average event duration was 4.1 ± 4.7 h (range: 1–38 h). The average time between events was 22 ± 27 h (range: 4–177 h), indicating that there was typically one event per day.

4.2. Throughfall and stemflow

Throughfall (*TF*) was measured approximately every 2–3 days on 155 occasions between 28 November 2000 and 29 October 2001 (except for the period 9 March–16 March 2001). Total *TF* was 1631 mm, or 74% of the corresponding P of 2198 mm. The standard error (SE) of the total *TF* was 4.5% (i.e. 73 mm or 3.3% of P). Further information about these measurements and the sampling errors can be found in Holwerda et al. (2006).

The time between two successive *TF*-readings varied between zero and 11 days (2.4 days on average). As a result, the number of P events that accumulated during each measuring interval ranged from 1 to 10 (2.2 events on average, cf. Fig. 2). On 17 occasions, rainfall started during the measurement of *TF*, requiring the results for such events to be split between two successive *TF*-samplings (Fig. 2). The data for these sampling occasions were merged, thereby reducing the total number of *TF*-sampling occasions from 155 to 138.

Average stemflow (*SF*) per tree species was estimated at 0.3% of P for *D. excelsa*, 0.6% for *S. berteriana*, 2.7% for *P. montana*, and <0.1% for *C. peltata*. The *SF* associated with the other main species in this forest was estimated at 0.5% of P (Scatena, 1990). Adding the latter value to those measured by the present study gave an estimated species-weighted *SF* of about 4% at the stand level. The SE of the *SF* estimate was about 42% (i.e. 1.7% of P); see Holwerda et al. (2006) for details.

4.3. Rainfall interception loss: observations and modeling

Total interception loss (I) was 474 mm (22% of the corresponding P of 2198 mm). Adding the SE's of the total *TF* and *SF* quadratically would suggest an SE of 82 mm (i.e. 4% of P) for I. Fig. 3a shows a scatter graph of I versus P for all 138 sampling occasions, demonstrating the fairly close overall correlation between the two variables ($r^2 = 0.75$). However, for sampling occasions with $P > 60$ mm, the scatter was substantial and produced a negative value when determining the canopy storage capacity (S) using Eq. (10). Therefore, the few sampling occasions with $P > 60$ mm ($n = 5$) were excluded from the present analysis. In addition, sampling occasions for which the SE of the *TF* measurement (SE_{TF}) exceeded the I estimate ($n = 12$) were also omitted, leaving a total of 121 sampling occasions (88% of the data) to be analyzed (see zoom in Fig. 3a). Total I for the selected sampling occasions was 389 mm (or 26% of the corresponding P of 1472 mm). The strong linear relationship between I and P ($I = 0.21(\pm 0.01)P + 0.60(\pm 0.17)$, $r^2 = 0.82$) indicates that there was substantial evaporation from the wetted canopy. The plus/minus values are the SE's of the regression coefficients.

For the derivation of the Gash model parameters, only sampling occasions that included a single P event were used ('calibration' data-set, cf. Fig. 2). The stem storage capacity (S_t) was estimated at 0.14 mm by adding the (negative) y-intercepts of the regressions between P (mm) and *SF* volume (L) for each of the four measured species, multiplied by the respective stem densities (m^{-2}). The *SF* fraction (p_t) was estimated at 0.05 from the slopes of the regressions between P and *SF*, multiplied by stem density (including the estimate for other species; Holwerda et al., 2006).

Fig. 3b shows I versus P for the calibration data-set ($n = 51$). The rainfall required to saturate the canopy (P') was determined at 0.72 mm. The linear regression equation linking I and P (both in mm) for $P < P'$ was $I = 0.72P$ ($r^2 = 0.97$, $n = 5$), giving a value of 0.23 for p (Eq. (9b)). The corresponding relationship obtained for $P \geqslant P'$ was $I = 0.20(\pm 0.02)P + 0.37(\pm 0.15)$ ($r^2 = 0.77$, $n = 46$), yielding $\overline{E}/\overline{R} = 0.20 \pm 0.02$ (SE) and $S = 0.37 \pm 0.15$ (SE) mm (Eq. (10)). The use of a larger value for P' (2 mm) gave identical results for S and $\overline{E}/\overline{R}$, but a much higher value for p (0.50). However, accounting for the lower evaporation rate occurring during canopy wetting (Gash, 1979; cf. Klaassen et al., 1998) increases the value of S by only 17% to 0.43 mm. As indicated by the respective 95% confidence intervals, the uncertainty in S (0.07–0.68 mm) is much higher than that in $\overline{E}/\overline{R}$ (0.16–0.24).

The performance of the analytical interception model was tested using the data from the sampling occasions that included two or more P events ('validation' data-set, Fig. 2). Fig. 3c shows observed and modeled I versus P for the validation data-set ($n = 70$). Predicted values of I agreed well with observations, with total modeled I (326 mm) being 7% higher than measured I (305 mm). The regression of modeled (y) against measured $I(x)$ was $y = 0.93x + 0.61$ (mm) ($r^2 = 0.84$, $n = 70$); the root mean squared error (RMSE) was 1.41 mm.

The sensitivity of the model results to changes in S and the average evaporation rate ($\overline{E}$) is explored in Fig. 4. The slope (a) and intercept (b), and the coefficient of determination (r^2) of the linear regression of modeled against measured I for the validation data-set were used as efficiency criteria. The better the agreement between modeled and measured I, the closer the value of b is to zero,

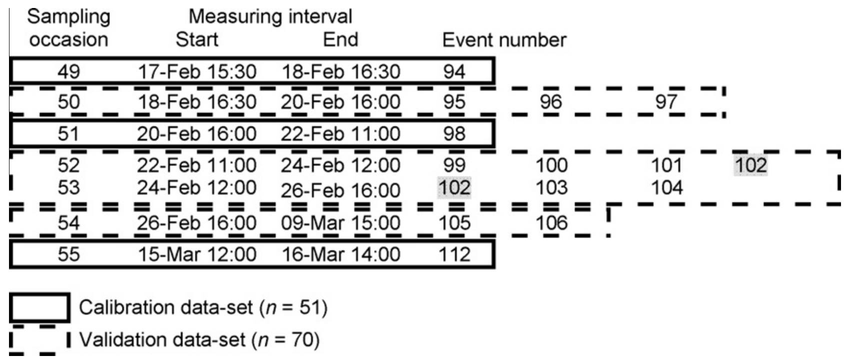

Fig. 2. For each *TF*-sampling occasion (numbers to the left; n = 155 in total), an inventory of the rainfall events that occurred in the measuring interval was made (numbers to the right). A total of 17 pairs of two consecutive *TF*-samplings shared a *P* event because rainfall occurred whilst *TF* was being measured (e.g. samplings 52 and 53 share event 102). The data from each of these pairs were merged, reducing the total number of sampling occasions to 138. Seventeen of these were excluded from the current analysis (see text and Fig. 3), leaving a total of 121. For calibration of the interception model, only sampling occasions with a single rainfall event (samplings 49, 51, and 55 in this example) were used (n = 51 in total). For validation of the model, data from sampling occasions containing more than one rainfall event were used (samplings 50 and 54), including those that were merged (samplings 52 and 53; n = 70 in total). See text for further explanation.

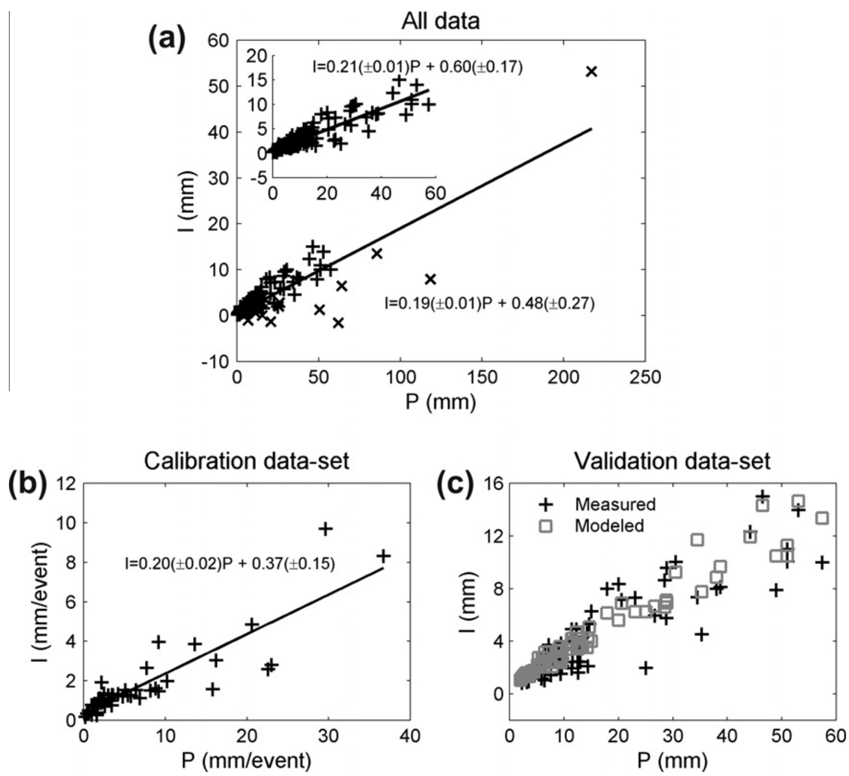

Fig. 3. (a) Rainfall interception (*I*) versus rainfall (*P*) for all 138 *TF*-sampling occasions (Fig. 2). The zoom shows the data that were used in the present analysis (n = 121 sampling occasions). Crosses represent data with $P > 60$ mm or $SE_{TF} > I$ and were left out of the analysis (n = 17 sampling occasions). The regression equations are: $I = 0.19(\pm0.01)P + 0.48(\pm0.27)$ (mm), $r^2 = 0.75$ (all data); and $I = 0.21(\pm0.01)P + 0.60(\pm0.17)$ (mm), $r^2 = 0.82$ (selected data). The plus/minus values are the standard errors (SE) of the regression coefficients. (b) *I* versus *P* based on the calibration data-set (n = 51; line shown is Eq. (10a)). (c) Idem for the validation data-set (n = 70). See Fig. 2 and text for further explanation.

and the closer the values of a and r^2 are to unity. Fig. 4 shows that the best fit was obtained for a combination of low S and high $\overline{E}$. Whilst increasing S and decreasing $\overline{E}$ will give a value of a that is very similar to that obtained with the current values of S and $\overline{E}$ (a = 0.93, see above), the corresponding values of b and r^2 would increase and decrease, respectively, indicating a poorer overall fit between modeled and measured I.

Estimating the average wet-canopy evaporation rate $\overline{E}$ from $\overline{E}/\overline{R}$ (0.20 ± 0.02, Eq. (10); cf. Fig. 3b) and average rainfall rate onto a saturated canopy $\overline{R}$ (3.16 mm h^{-1}) gave a value for $\overline{E}$ of 0.63 ± 0.06 mm h^{-1} (Table 2).

4.4. Quality of the turbulence data

Between November 2000 and October 2001 there were a total of 724 h with $P > 0.5$ mm. Eddy covariance and other micrometeorological data for calculating E were available for 553 of these hours (76% of the data). The performance of the sonic anemometer during rainfall was tested by plotting the standard deviation of vertical wind speed (σ_w) against friction velocity (u_*) for hours with $P > 0.5$ mm and near-neutral atmospheric conditions (Fig. 5a; Gash et al., 1999; Van der Tol et al., 2003). According to Monin–Obukhov similarity theory, the ratio of σ_w to u_* under neutral conditions is

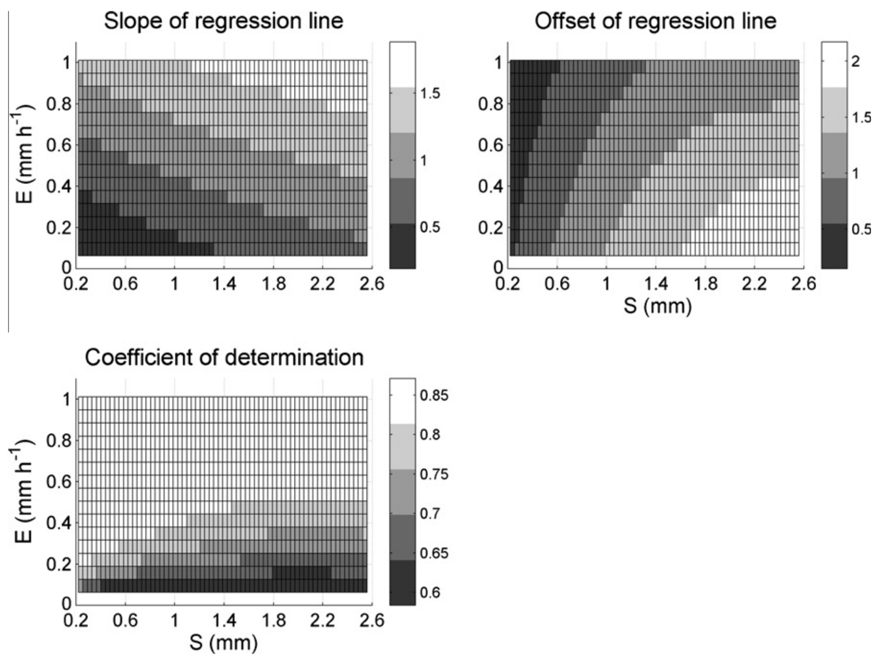

Fig. 4. The regression coefficients and coefficient of determination of the linear regression of modeled against measured interception loss (validation data-set) for different combinations of the canopy storage capacity (S) and wet canopy evaporation rate ($\overline{E}$).

Table 2
Average wet-canopy evaporation rates ($\overline{E}$, mm h^{-1}) as derived from the throughfall data and calculated using: (i) the Penman–Monteith equation with the aerodynamic conductance ($g_{a,M}$) calculated with Eq. (2) using wind speed data from the lower (lee-side) Bisley tower; (ii) idem using wind speed data from the upper, more exposed tower; (iii) the P–M equation with measured (eddy covariance) $g_{a,M}$; and (iv) the energy balance equation and sensible heat flux measured by the sonic anemometer. Only hours with $P > 0.50$ mm were assumed to represent wet canopy conditions ($n = 553$ h). Also shown are the corresponding average rainfall rate ($\overline{R}$, mm h^{-1}) and relative evaporation rate ($\overline{E}/\overline{R}$).

Method	$\overline{E}$ (mm h^{-1})	$\overline{R}$ (mm h^{-1})	$\overline{E}/\overline{R}$ (–)
Throughfall (observed)	0.63 ± 0.06	3.16	0.20 ± 0.02
P–M, $g_{a,M}$ calculated, lower tower	0.16		0.05
P–M, $g_{a,M}$ calculated, upper tower	0.40		0.13
P–M, $g_{a,M}$ measured	0.58		0.18
Eddy covariance	0.13		0.04

constant, and thus the relationship between the two variables should be linear (Garratt, 1992; cf. Gash et al., 1999; Van der Tol et al., 2003). As shown in Fig. 5a, there is a strong linear relation between σ_w and u_*, suggesting good performance of the sonic anemometer. The good agreement between the ITC for rainy and dry conditions also indicates that the quality of the turbulence measurements was not affected by the rain (Fig. 5b–d).

Fig. 5b–d shows that for the vertical wind component (w) and temperature (T_s) the observed ITC were higher than the theoretical values, whereas for the horizontal wind component (u) measured values were lower than predicted. The proportion of data for which the difference between measured and predicted ITC exceeded 30% was 45% and 38% for w and T_s, respectively, but less than 1% in the case of u.

The stationarity test showed that the SD of the hourly mean momentum ($\overline{w'u'}$ and $\overline{w'v'}$) and sensible heat ($\overline{w'T'_s}$) fluxes were typically 1–2 times the mean values. For <1% of the momentum and sensible heat flux data, the SD was <30% of the mean, suggesting that the assumption of stationarity was almost never met (see Section 5).

4.5. Comparison of Penman–Monteith- and eddy covariance-based estimates of evaporation with observations

The average E rates calculated with the Penman–Monteith (P–M) equation (using different methods for calculating $g_{a,M}$) and that derived using the energy balance equation and the sensible heat flux measured by the sonic anemometer are listed in Table 2. The P–M-based rate using measured $g_{a,M}$ (0.58 mm h^{-1}) was very similar to the *TF*-based evaporation rate of 0.63 mm h^{-1}. The corresponding value of $g_{a,M}$ was 0.31 m s^{-1}. However, when $g_{a,M}$ was calculated with Eq. (2) using wind data from the lower Bisley tower, the P–M-based $\overline{E}$ was about 75% lower (0.16 mm h^{-1}) than the observed $\overline{E}$; better results were obtained ($\overline{E} = 0.40$ mm h^{-1}) with $g_{a,M}$ estimated using wind data from the upper Bisley tower. Corresponding values of $g_{a,M}$ were 0.05 and 0.21 m s^{-1}, respectively, the difference reflecting the higher wind speeds measured at the upper tower (ca. 4.0 versus ca. 1.0 m s^{-1} at the lower tower; see also Fig. 7c below). $\overline{E}$ calculated from the energy balance equation and H_s was only 0.13 mm h^{-1}, and almost 80% lower than the throughfall-based $\overline{E}$. Corresponding values of H_s were -20 ± 37 W m^{-2} on average (equivalent to about -0.03 mm h^{-1}) and negative for 80% of the time. The minimum value of H_s observed was -140 W m^{-2} (equivalent to about -0.21 mm h^{-1}).

Fig. 6a shows a plot of the interception fraction (I/P) versus P. To limit the cumulative effect of having multiple storms during a sampling interval, only sampling occasions with a maximum of three events were used ($n = 101$). I/P decreased with increasing P for totals up to about 10 mm. For $10 < P < 30$ mm, there was no clear relationship ($I/P = 0.24 \pm 0.10$ (SD); $n = 26$), but for $P > 30$, the variability decreased and I/P values appeared to converge to ~0.2.

In the present case, where the canopy storage capacity is small ($S = 0.37$ mm) and the relative evaporation rate large ($\overline{E}/\overline{R} = 0.20$), the value of I/P for $P > 10$ mm largely reflects evaporation from the saturated canopy (cf. Table 1). Hence, part of the variation in observed I/P values may have been caused by variation in $\overline{E}/\overline{R}$. To investigate this further, values of $\overline{E}/\overline{R}$ were derived for each sampling occasion, again using the P–M- and eddy covariance-based

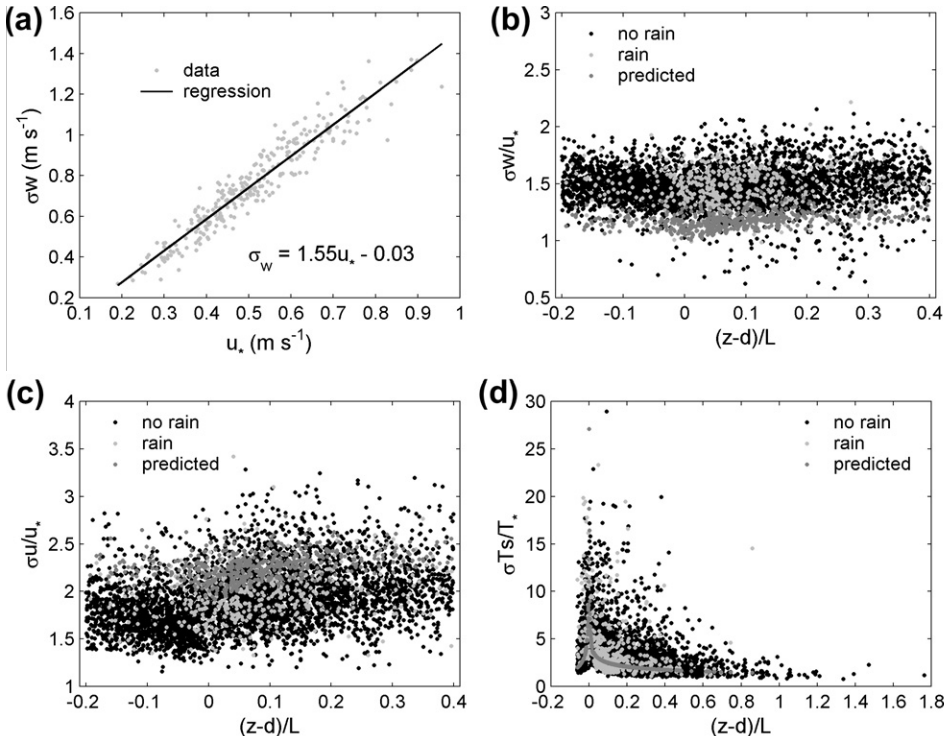

Fig. 5. (a) Hourly averages of the standard deviation of vertical wind speed (σ_w, m s^{-1}) against friction velocity (u_*, m s^{-1}) for wet-canopy ($P > 0.50$ mm h^{-1}) and near-neutral ($-0.1 < (z-d)/L < 0.1$) conditions. The regression equation reads: $\sigma_w = 1.55u_* - 0.03$ (m s^{-1}), $r^2 = 0.90$, $n = 271$ h. (b–d) The integral turbulence characteristics (ITC) of the vertical (w) and horizontal (u) wind components and temperature (T_s) as a function of atmospheric stability ($(z-d)/L$) for rainy and dry conditions. Theoretical values were calculated following Thomas and Foken (2002).

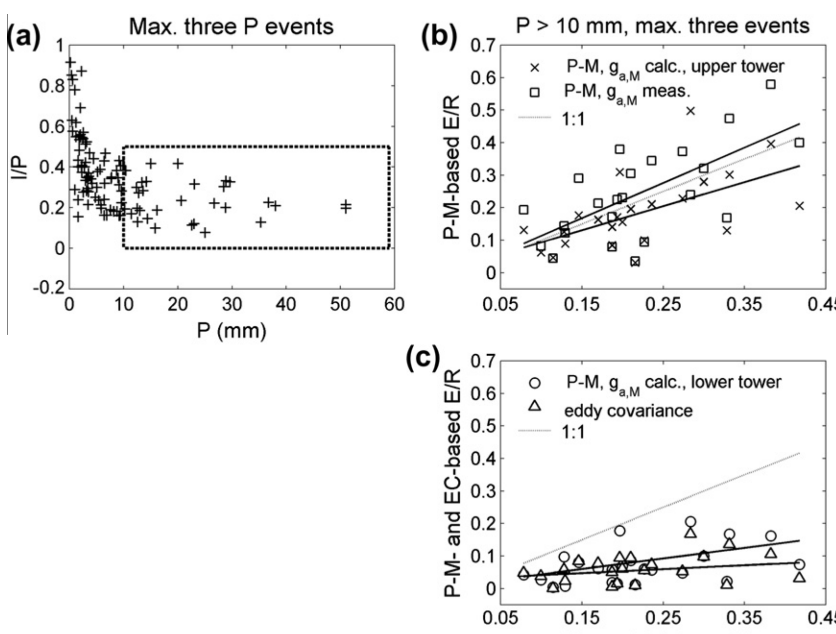

Fig. 6. (a) The interception fraction (I/P) against rainfall (P) for *TF*-sampling occasions that included ⩽three P events ($n = 101$). (b) The Penman–Monteith-based relative evaporation rate ($\overline{E}/\overline{R}$), with $\overline{E}$ calculated using either measured aerodynamic conductance ($g_{a,M}$) (eddy covariance) or derived with Eq. (2) using wind data from the upper (exposed) Bisley tower, versus the *TF*-based interception fraction for $P > 10$ mm (as highlighted by the square within the left-hand panel). The regression equations are: (P–M, $g_{a,M}$ measured) $\overline{E}/\overline{R} = 1.06(\pm0.26)I/P + 0.01(\pm0.06)$, $r^2 = 0.45$; and (P–M, $g_{a,M}$ calculated, upper tower) $\overline{E}/\overline{R} = 0.74(\pm0.22)I/P + 0.02(\pm0.05)$, $r^2 = 0.35$. (c) Idem with $g_{a,M}$ obtained from Eq. (2) using wind data from the lower (lee-side) tower and with $\overline{E}$ calculated using the energy balance equation and the sensible heat flux measured by the sonic anemometer. The regression equations are: (P–M, $g_{a,M}$ calculated, lower tower) $\overline{E}/\overline{R} = 0.29(\pm0.13)I/P + 0.01(\pm0.03)$, $r^2 = 0.20$; and (eddy covariance) $\overline{E}/\overline{R} = 0.16(\pm0.10)I/P + 0.03(\pm0.02)$, $r^2 = 0.11$. The plus/minus values are the standard errors (SE) of the regression coefficients.

E rates. The respective results are compared with the corresponding *TF*-based I/P values in Fig. 6b and c. For eight out of 31 sampling occasions with $P > 10$ mm, micrometeorological data were missing, limiting the comparison to 23 occasions (74% of the data). The best agreement between $\overline{E}/\overline{R}$ and I/P was (again) obtained when E was calculated with the P–M equation using measured $g_{a,M}$

(slope = 1.06 ± 0.26 (SE), Fig. 6b). Using calculated $g_{a,M}$ (Eq. (2)) in the P–M equation, the fit was reasonable when using wind data from the (exposed) upper Bisley tower (slope = 0.74 ± 0.22, Fig. 6b), but poor when using data from the lower tower (slope 0.29 ± 0.13, Fig. 6c). Agreement with the observations was also very poor when E was derived using the energy balance equation and H_s (slope = 0.16 ± 0.10, Fig. 6c).

4.6. Diurnal variations in interception rate

As shown in Fig. 6, there was considerable variation in I/P for $P > 10$ mm. Some of this variation must have been caused by differences in the number of events occurring per sampling interval (between one and three) and by sampling errors in the *TF* measurements. However, the results suggest that almost half of the total variability was caused by variations in the relative evaporation rate (Fig. 6b). The average diurnal patterns for $\overline{E}/\overline{R}$ and for various closely associated variables are shown in Fig. 7. It should be noted that only E values calculated using measured $g_{a,M}$ were used in the analysis.

Rainfall intensities (R) were higher in the afternoon and early night than during the late night and morning, reflecting the dominance of convective and orographic rainfall, respectively. Despite the fact that only hours with $P > 0.5$ mm (i.e. saturated canopy conditions) were used in the calculations, the mean vapor pressure deficit (*VPD*) during the day (0.26 kPa) was almost 1.4 times that observed at night (0.19 kPa) (Fig. 7b). Part of this difference will probably have been caused by the higher temperatures during the day (22.5 °C versus 21.8 °C at night), but other factors (such as e.g. depth of the boundary layer) may also have played a role. Mean net radiant energy inputs during the day (R_n) were low (156 W m^{-2}, equivalent to about 0.23 mm h^{-1}).

Although wind speed (u) at the more exposed upper Bisley tower was almost four times that measured at the lower tower, neither site showed a marked diurnal variation in wind speeds during wet-canopy conditions (Fig. 7c). Wind direction (U_{dir}) at the lower tower followed a pattern that was also observed under non-rainy conditions, i.e. upslope (northerly) winds during the day and downslope (southerly) winds at night; no such diurnal variation in U_{dir} was observed at the upper tower site (Fig. 7d). The average friction velocity (u_*) was 0.48 m s^{-1} during the day and 0.42 m s^{-1} at night (Fig. 7e). Because the pattern of u_* largely coincides with that of U_{dir} (Fig. 7e and d), the observed change in u_* may reflect a change in surface roughness. However, differences in atmospheric stability may also play a role. In any case, because of the higher daytime values of u_* (for equal u), the ratio u_*/u, and consequently $g_{a,M}$ (Eq. (3)), was higher during the day (0.36 m s^{-1} on average) than at night (0.27 m s^{-1}) (Fig. 7f).

Because of the higher R_n, *VPD*, and $g_{a,M}$ during the day, the corresponding average rate of E (0.86 mm h^{-1}) was about 2.5 times the night-time value (0.34 mm h^{-1}) (Fig. 7g). Consequently, $\overline{E}/\overline{R}$ was also higher during the day (0.27) than at night (0.12) (Fig. 7h). Interestingly, the (convective) rainfall intensity peaks in the early afternoon and early night (Fig. 7a) corresponded with lowered $\overline{E}/\overline{R}$ values during these periods (Fig. 7h).

The higher values of E and $\overline{E}/\overline{R}$ obtained for daytime conditions (Fig. 7g and h) suggest that interception losses may be higher during the day than at night. Therefore, all sampled intervals were assigned to daytime or night-time occurrence (based on average R_n during the events). Considering all data, there was no significant difference in average I/P between daytime (0.33 ± 0.14) and night-time (0.31 ± 0.13) data (Table 3). Possibly, the effect of higher $\overline{E}/\overline{R}$ values during the day is (partly) offset by the occurrence of

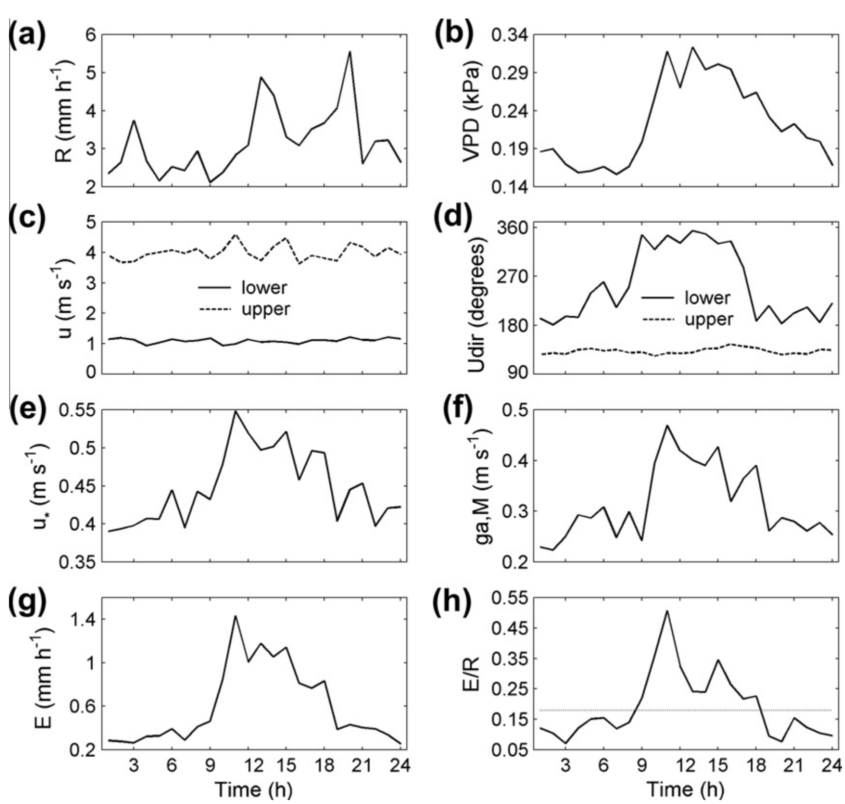

Fig. 7. Average daily patterns at the Bisley forest site during wet-canopy conditions ($P > 0.50$ mm h^{-1}) of: (a) rainfall intensity (R, mm h^{-1}); (b) vapor pressure deficit (*VPD*, kPa); (c) wind speed (u, m s^{-1}); wind speed measured at the upper tower is also shown for comparison; (d) wind direction (U_{dir}, degrees); U_{dir} measured at the upper tower is also shown for comparison; (e) friction velocity (u_*, m s^{-1}); (f) (eddy covariance-based) aerodynamic conductance ($g_{a,M}$ m s^{-1}); wet-canopy evaporation (E, mm h^{-1}); and (h) relative evaporation rate ($\overline{E}/\overline{R}$) (dotted line is the average value of 0.18).

Table 3
The total number of throughfall-sampling occasions (n), total rainfall (P, mm), total interception loss (I, mm), and average interception fraction (I/P) for all *TF*-sampling occasions that included up to a maximum of three P events (n = 101), separately for day- and night-time conditions (average net radiation R_n larger than and smaller than zero, respectively) and P size (P > 10 mm). Please note that seven sampling occasions were left out of the analysis because R_n data were not available. See text for further explanation.

	All data (max. three events)				P > 10 mm (max. three events)			
	n	P	I	I/P (±SD)	n	P	I	I/P (±SD)
Daytime	60	739	196	0.33 ± 0.14	24	559	135	0.25 ± 0.09
Night-time	34	224	56	0.31 ± 0.13	6	103	20	0.20 ± 0.08

smaller storms at night (on average 6.6 mm per sampling occasion) than during the day (12.3 mm on average). For P > 10 mm, the difference in I/P between daytime (0.25 ± 0.09) and night-time (0.20 ± 0.08) was larger, but again not significant (Table 3).

5. Discussion

5.1. Coastal proximity versus topographically enhanced roughness

The results of the present study confirm the high rainfall interception determined earlier for the Bisley forest (Schellekens et al., 1999, 2000; cf. Scatena, 1990). The results also indicate that the previously reported discrepancy between throughfall-based and calculated (Penman–Monteith equation) wet-canopy evaporation rates at this site (Schellekens et al., 1999, 2000) is most likely due to underestimation of the aerodynamic conductance ($g_{a,M}$), as calculated from vegetation properties alone (Eq. (2)).

Eq. (2) is a semi-empirical relationship that is valid for flat terrain with an extensive, uniform vegetation cover (e.g. Monteith and Unsworth, 2008). It predicts $g_{a,M}$ based on measured wind speed and inferred values for the zero-plane displacement and roughness length (Thom, 1975), which are conventionally estimated from forest height (Rutter et al., 1971, 1975; cf. Shuttleworth, 1988, 1989). In doing so, it is implicitly assumed that the similarity theory for the transfer of momentum can be applied even relatively close to the forest surface, regardless of the prevailing topography. As such, it is of interest to examine to what extent this assumption is valid in practice.

Van der Tol et al. (2003) compared values of $g_{a,M}$, as calculated using Eq. (2), with values measured by sonic anemometry (Eqs. (3) and (4)) for a 15 m tall Sitka spruce forest on a gentle (5.7°) slope in central Wales (UK). Overall, the difference between average measured (0.22 m s^{-1}) and calculated (0.18 m s^{-1}) $g_{a,M}$ was small (at u = 2.8 m s^{-1}). However, when compared per wind direction sector, measured values varied between 0.5 and 1.6 times the calculated ones (Van der Tol et al., 2003). Similarly, for a 22 m tall (mixed) deciduous forest in southern England, Herbst et al. (2008) reported average values of measured and calculated $g_{a,M}$ of 0.11 versus 0.16 m s^{-1}, respectively (at u = 3.1 m s^{-1}), for the leafed period, and 0.17 versus 0.16 m s^{-1}, respectively (at u = 4.2 m s^{-1}), for the leafless periods. Finally, for a 35 m tall lowland rain forest in gently undulating terrain in central Amazonia, Lloyd et al. (1988) obtained average values of 0.029 m s^{-1} and 0.034 m s^{-1} for $g_{a,M}$ based on eddy covariance measurements and Eq. (2), respectively (at u = 1.0 m s^{-1}; see also Shuttleworth, 1988). The latter values are identical to that derived by Kume et al. (2008) for a 40–50 m tall lowland rain forest in Borneo located on a gentle (<5°) slope (0.03 m s^{-1}, again at u = 1 m s^{-1}), using values for zero-plane displacement and roughness length derived from wind profiles.

By contrast, in the present study, measured values of $g_{a,M}$ (0.31 m s^{-1} on average) were almost six times those predicted using Eq. (2) (0.05 m s^{-1}; at $u \approx 1$ m s^{-1}). Although the higher value of $g_{a,M}$ calculated using wind data from the upper Bisley tower (0.21 m s^{-1} on average) suggests that Eq. (2) may yield better estimates of $g_{a,M}$ at exposed sites, direct measurements of $g_{a,M}$ at the upper Bisley tower site are needed to establish to what extent this is the case. Nevertheless, the presently found difference between measured and calculated $g_{a,M}$ is much greater than observed by Lloyd et al. (1988), Van der Tol et al. (2003), and Herbst et al. (2008). Arguably, the main difference between the present site and these other studies relates to their topographic setting, i.e. complex (mountainous) versus gentle terrain. Indeed, the much higher average value of $g_{a,M}$ measured in the Bisley study (0.31 m s^{-1}) compared to those measured by Lloyd et al. (1988) in Amazonia (10 times lower), by Van der Tol et al. (2003) in Wales (almost four times lower), and by Herbst et al. (2008) in southern England (almost 10 times lower) strongly suggests that the complex topography of the Luquillo Mountains increases the efficiency of the turbulent (energy) exchange compared to sites located in gentler terrain (note that these values of $g_{a,M}$ were scaled to values at u = 1 m s^{-1}). Similarly high values for $g_{a,M}$ (at u < 1 m s^{-1}) have been estimated by Asdak et al. (1998a) (0.31 m s^{-1}) and by Vernimmen et al. (2007) (~0.45 m s^{-1}) for 40–50 m tall lowland rain forests situated in dissected hilly terrain (with slopes up to 35°) in central Kalimantan (Indonesia), based on an inverse application of the Penman–Monteith equation and throughfall-based interception rates.

The high $g_{a,M}$ measured at the Bisley site and the high values that were indirectly derived at the two sites in central Kalimantan (Asdak et al., 1998a; Vernimmen et al., 2007) are to be expected for measurements over forests in rugged terrain. In such environments, wind profile observations (see survey of Chen and Schwerdtfeger (1989)) show that the measurement level is contained within the friction layer, where $g_{a,M}$ is always enhanced (see Section 2). The similarity breakdown at measurement level is also reflected by the relatively high σ_w/u_* ratio (Fig. 5a and b) obtained in the present study. According to Monin–Obukhov similarity theory, σ_w/u_* in neutral atmospheric conditions is a universal constant, with observed values over uniform areas typically close to 1.25 (Panofsky et al., 1977; Garratt, 1992; cf. Gash et al., 1999). A similarly high value for σ_w/u_* (~1.5) was observed by Van Gorsel et al. (2003) over complex topography in the Alps.

More work is required to understand more fully the observed spatial variation in $g_{a,M}$ (Fig. 7f; cf. Van der Tol et al., 2003). Measured values of $g_{a,M}$ are representative of the source area(s) sampled by the sonic anemometer (usually a couple of hundred meters upwind of the instrument; e.g. Schuepp et al., 1990). At Bisley, $g_{a,M}$ varied with wind direction (Fig. 7f and d). This is apparently caused by the corresponding changes in surface roughness (cf. Van der Tol et al., 2003), but differences in atmospheric stability (e.g. between daytime and night-time conditions) may also have played a role. Similarly, part of the variation in measured and differently calculated rates of E shown in Fig. 6b may also have been caused by differences in the magnitude of the momentum fluxes over the source area(s) of the sonic anemometer and those experienced at the throughfall plot.

It has been hypothesized that wet-canopy evaporation rates (E) under maritime tropical conditions are higher than at mid-continental sites (Shuttleworth, 1989; Schellekens et al., 2000; cf. Roberts et al., 2005). Table 4 brings together a selection of tropical interception studies for which *TF*-based and calculated (Penman–Monteith) values of E have been derived. Indeed, at 23 ± 7% versus 12 ± 3%, the average interception ratio (I/P) is almost two times higher for the 'maritime' contingent (n = 8, excluding the exceptionally high value derived for the presently studied forest by previous researchers) than for the continental sites (n = 5). However, the average observed (TF-based) evaporation rate is nearly equal for the maritime and continental studies (0.50 ± 0.20 mm h^{-1} versus 0.50 ± 0.23 mm h^{-1}, respectively; Table 4), whereas calculated values of E are somewhat lower for the former than for the latter (0.18 ± 0.06 mm h^{-1} versus 0.24 ± 0.08 mm h^{-1}, respectively). As such, at present the limited number of studies suggest there is no clear pattern of consistently enhanced E under maritime conditions, and the higher I/P under maritime conditions may well in part reflect the lower prevailing rainfall intensities (4.3 ± 1.0 mm h^{-1} on average versus 6.5 ± 1.6 mm h^{-1} (excluding the very high value of 20 mm h^{-1} from Ivory Coast) for the continental sites; Table 4; cf. Scatena, 1990).

However, the data in Table 4 may also be interpreted in terms of contrasts in topographic setting between sites. It is pertinent to note that the sites situated in more mountainous and dissected terrain within the maritime group (Puerto Rico, Brunei, Fiji) tend to show enhanced TF-based E compared to their counterparts located in gentler terrain (West Java, Sarawak, coastal Queensland). A similar pattern is observed for the continental group, with higher values of TF-based E at sites with a more dissected topography (Table 4), although an extension of the analysis using data for a larger number of sites is needed.

5.2. Sources of energy maintaining high rates of wet-canopy evaporation

The values of E that greatly exceed the rates sustained by net radiant energy alone indicate that the high rates of wet-canopy evaporation observed at Bisley (and other sites) are driven by a negative (downward) sensible heat flux (e.g. Stewart, 1977; Shuttleworth and Calder, 1979; Blyth et al., 1994; Asdak et al., 1998a; see also discussion in Roberts et al., 2005). The fact that the sensible heat flux measured above the Bisley forest (H_s, Eq. (6)) was negative for almost 80% of the time during saturated canopy conditions seems to confirm this. However, at the same time the value of E derived from the energy balance equation (Eq. (5)) and H_s was much too low (Table 2, Fig. 6c), suggesting that H_s was strongly underestimated.

A possible explanation for this underestimation of H_s is that the exchange of sensible heat during rainfall at Bisley occurred during specific (intermittent) events, as indicated by the non-stationarity of the flux data (see Section 3). Acevedo et al. (2006) showed that under intermittent conditions the use of a fixed and very short flux-averaging time, such as the 5-min intervals used in the present study, can result in a strong underestimation of H_s. They proposed to use a variable flux-averaging time to better represent the different time scales of intermittent events. Similarly, Finnigan et al. (2003) showed that in the case of forests with complex topography, low frequency motions make a large contribution to the total flux. Naturally, these low frequency fluxes are entirely lost when using a 5-min averaging period.

To quantify the intermittency of the turbulence during rainfall at Bisley, an intermittency factor (IF) for H_s was calculated for each rainfall event. First, the 5-min values of H_s observed during a particular event were sorted (in ascending order). Next, IF was obtained as the fraction of the total time required to attain 50% of the total H_s during that particular event (Acevedo et al., 2006). Under well-developed turbulent conditions, H_s is equally distributed over time, and hence, the value of IF is close to 0.5. If, however, the turbulence is intermittent and most of H_s takes place during specific events, IF approaches zero (Acevedo et al., 2006). Considering only events with $P > 10$ mm, the average IF for H_s was 0.15 ± 0.07 (SD) (range: 0.01–0.26). Clearly, more work is needed to better quantify the sensible heat exchange under rainy

Table 4
Results obtained by selected rainfall interception studies conducted under 'maritime' and 'continental' tropical climatic conditions. Studies were selected on the basis of the availability of throughfall-based measurements of wet-canopy evaporation ('Observed E'), and of rates calculated with the Penman–Monteith equation ('Calculated E'). Also listed are the interception fraction (I/P), the average rainfall rate (R), and an indication of local topography (see text for explanation).

Site	Topography, distance to coast	I/P (%)	Observed E (mm h^{-1})	Calculated E (mm h^{-1})	R (mm h^{-1})	Reference
'Maritime' sites						
Luquillo, Puerto Rico	Mountainous, ~10 km	50	1.03	0.11	3.0	Scatena (1990), Schellekens et al. (1999, 2000)
Idem	Idem	27	0.63	0.20	3.2	This study
Brunei, Borneo	Mountainous, 20–25 km	18	0.71	0.20	5.5	Dykes (1997)
West Java, Indonesia	Undulating, 45 km	22	~0.19	0.17	>5?	Calder et al. (1986)
Sarawak, East Malaysia	Gentle slope, 17 km	12	~0.42	–	5.0	Kumagai et al. (2005), Manfroi et al. (2006)
Oliver Creek, north Queensland, Australia	Gentle slope, 1 km	26	0.35	0.24	4.6	Wallace and McJannet (2008)
Hutchinson Creek, north Queensland, Australia	Gentle slope, 3 km	25	0.45	(0.24)	4.0	Wallace and McJannet (2008)
Mt. Lewis I, north Queensland, Australia	Sloping, 25 km	35	0.46	(0.06)[a]	3.2	Wallace and McJannet (2008)
Tulasewa, Viti Levu, Fiji	Dissected hills, 15 km	19	0.72	0.18	5.5	Waterloo (1994), Waterloo et al. (1999)
'Continental' sites						
Ducke, Manaus, Amazonia, Brazil	Plateau	9	–	0.21	5.2	Lloyd et al. (1988)
Cuieiras, Manaus, Amazonia, Brazil	Plateau	13[b]	0.32[c]	0.31	8.8[b]	Cuartas et al. (2007)
Barito Ulu, central Kalimantan, Indonesia	Dissected hills	16	0.82	0.17	6.6	Vernimmen et al. (2007)
Upper Mentaya, central Kalimantan, Indonesia	Rolling	11	0.51	0.30	5.5	Asdak et al. (1998a,b)
Tai, Ivory Coast	Gently undulating	9	0.34	0.18	20	Hutjes et al. (1990)

[a] Considered an underestimate by the authors themselves.
[b] Data for a year with normal rainfall.
[c] Measured by eddy covariance.

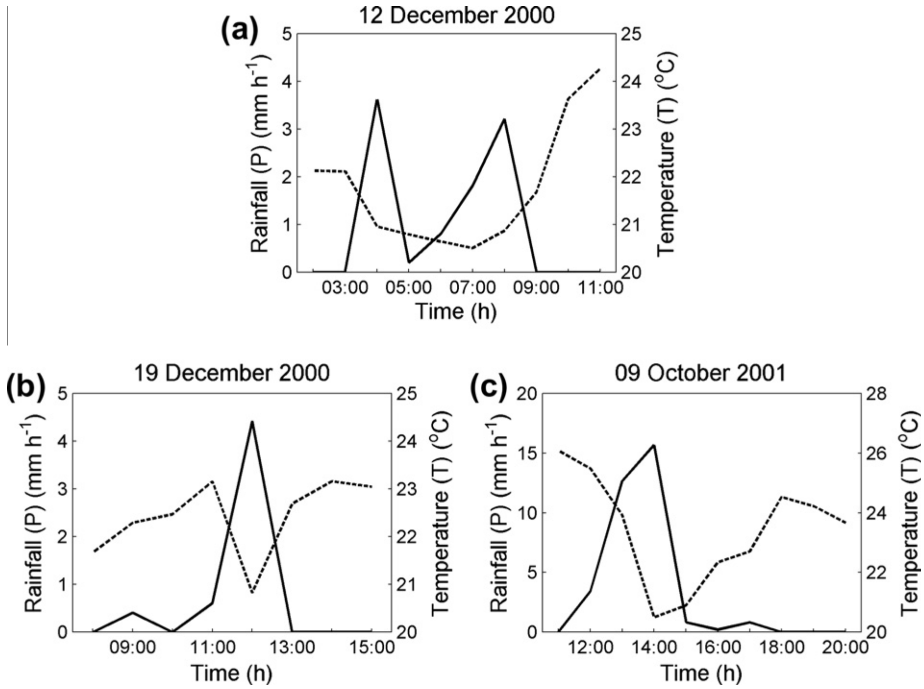

Fig. 8. Rainfall (P, mm h^{-1}; solid line) and temperature (T, °C; dashed line) for a night-time (a) and two daytime (b and c) rainfall events at the Bisley forest, Puerto Rico.

conditions at Bisley. Such work should include the collection of high frequency sonic anemometer wind and temperature data to test the variable flux-averaging time approach of Acevedo et al. (2006).

Possible sources of energy sustaining interception evaporation are sensible heat stored in the atmosphere or released by the condensation of water vapor higher up in the atmosphere (Shuttleworth and Calder, 1979). Wet-canopy evaporation at Bisley was higher during the day (0.86 mm h^{-1} on average) than at night (0.34 mm h^{-1}), partly due to the availability of radiant energy and higher aerodynamic conductance during the day (Fig. 7). Despite the fact that temperatures were lower during the night (implying a smaller availability of sensible heat for evaporation), the observed average night-time E of 0.34 mm h^{-1} must have involved a substantial downward heat flux (of about −230 W m^{-2} on average). Comparably high values of night-time evaporation were derived for a lowland rain forest setting in dissected terrain in central Kalimantan (Asdak et al., 1998a), but interestingly not for the lowland rain forests on the coastal plain of northern Queensland studied by Wallace and McJannet (2008).

A downward sensible heat flux will lead to atmospheric cooling (Watanabe and Mizutani, 1996) and the Bisley site is no exception. Fig. 8 shows the time series of rainfall and air temperature for a night-time (a) and two daytime (b and c) rainfall events. During the night-time event (12 December 2000), the air temperature decreased by ∼1.5 °C from about 22.1 °C at the beginning of the storm to about 20.5 °C near the end. Even larger drops in temperature were observed for the daytime events on 19 December 2000 (∼2.4 °C) and 9 October 2001 (∼5.6 °C). It is not known how much of this cooling is the result of interception evaporation or evaporation of falling raindrops. In addition, heat is released upon condensation of water vapor higher in the atmosphere. Hence, the observed temperature changes only reflect the net effect of all these processes.

Murakami (2006, 2007) showed E to increase with increasing rainfall intensity R, and explained this observation by postulating evaporation of splash droplets that are produced when raindrops hit the canopy. Although the good agreement between observed (TF-based) and calculated (P–M equation with measured $g_{a,M}$) evaporation at Bisley (Fig. 6b) suggests otherwise, it cannot be ruled out that some splash droplet evaporation contributes to interception evaporation at this site. For sampling occasions with more than 10 mm of rainfall (Fig. 6a) and an average $R < 5$ mm h^{-1} ($n = 25$ out of 30, i.e. the majority of the data), there was only a very weak correlation between average interception rate (estimated as interception amount divided by the number of hours with more than 0.5 mm of rainfall), and average R ($r^2 = 0.07$). However, after including the five sampling occasions with $R > 5$ mm h^{-1}, the relation improved considerably ($r^2 = 0.48$), suggesting that splash droplet evaporation became more important at higher rainfall intensities (cf. Murakami, 2007; Dunkerley, 2009). Nevertheless, just like the ‘regular’ evaporation of intercepted water from the canopy, evaporation of splashed droplets (in the canopy air space) also consumes energy, and this cannot be maintained (at high rates) without (substantial) downward transport of sensible heat (Murakami, 2006).

Dunin et al. (1988) advanced a related (and as yet untested) hypothesis in which intense rain promotes extra ventilation of the forest canopy and hence more rapid evaporation. The added air circulation through the canopy could be the result of downward drag exerted by the falling rain drops, a mechanism known to arise in the convective structure of thunderstorm cells (Kamburova and Ludlam, 1966). This, in turn, might drive air into the canopy from above, and generate outflows around or beneath the canopy, thereby ventilating the space within the foliage and branches (Dunin et al., 1988; Dunkerley, 2009). More work is needed to test either hypothesis (see also discussion in Dunkerley, 2009).

6. Concluding remarks

The preliminary comparison of wet-canopy evaporation rates (E, both throughfall-based and computed with the Penman–Monteith equation using conventionally derived estimates of aerodynamic conductance, $g_{a,M}$) for ‘maritime’ and ‘continental’ tropical sites (Table 4) does not show a clear pattern of enhanced rates at maritime sites as postulated by Shuttleworth (1989) and Schellekens et al. (2000). Instead, in the light of the results of the present study, the data collated in Table 4 suggest the occurrence of enhanced rates of E to be primarily related to added aerodynamic roughness (i.e. high values of $g_{a,M}$) for sites located in topographically complex terrain.

At the same time, it is clear that more work is required to better understand forest–atmosphere interactions during rainfall in tropical areas, particularly those with complex topography. Interception studies in such environments should aim to include direct measurements of aerodynamic conductance (using eddy covariance) to obtain further comparative data and collect high frequency sonic anemometer wind and temperature data to test the variable flux-averaging time approach of Acevedo et al. (2006). Future work should also include boundary-layer profiles of temperature, humidity, and wind speed as well as wind direction, to obtain (further) insight into the mechanisms maintaining the downward transport of sensible heat to the forest (cf. Blyth et al., 1994). The alternative hypotheses advanced by Murakami (2006) and by Dunin et al. (1988) also merit experimental verification of the mechanisms of splash droplet evaporation and added canopy ventilation during high rainfall intensities, respectively.

Acknowledgements

This work was supported by a Grant from the Netherlands Foundation for the Advancement of Tropical Research (WOTRO, Grant No. W76-206). Additional support was provided by the Luquillo Critical Zone Observatory, the International Institute of Tropical Forestry (IITF), Rio Piedras, Puerto Rico, and the VU University (VUA), Amsterdam, The Netherlands. The paper was written whilst the senior author was supported by NSF Grant No. NSF/DEB 0746179 to Dr. Heidi Asbjornsen (Iowa State University), whose support is gratefully acknowledged. Hans Bakker and Ron Lootens (VUA), as well as Carlos Estrada, Gustavo Guzman, and Samuel Moya (IITF) are thanked for their great help at various stages of the project. Professor Han Dolman (VU University) provided useful comments on an earlier version of the manuscript. Further, the senior author likes to express his gratitude to Professor Jeffrey McDonnell (Oregon State University) for providing such an inspiring working environment during the writing of this paper. Finally, the helpful comments by three anonymous reviewers are gratefully acknowledged.

References

Acevedo, O.C., Moraes, O.L.L., Degrazia, G.A., Medeiros, L.E., 2006. Intermittency and the exchange of scalars in the nocturnal surface layer. Boundary-Lay. Meteorol. 119, 41–55.

Asdak, C., Jarvis, P.G., van Gardingen, P., 1998a. Evaporation of intercepted precipitation based on an energy balance in unlogged and logged forest areas of central Kalimantan, Indonesia. Agric. Forest Meteorol. 92, 173–180.

Asdak, C., Jarvis, P.G., van Gardingen, P., 1998b. Modelling rainfall interception in unlogged and logged forest areas of Central Kalimantan, Indonesia. Hydrol. Earth Syst. Sci. 2, 211–220.

Bernhofer, C., 1992. Estimating forest evapotranspiration at a non-ideal site. Agric. Forest Meteorol. 60, 17–32.

Blyth, E.M., Dolman, A.J., Noilhan, J., 1994. The effect of forest on mesoscale rainfall: an example from HAPEX-MOBILHY. J. Appl. Meteorol. 33, 445–454.

Brown, S., Lugo, A.E., Silander, S., Liegel, L., 1983. Research History and Opportunities in the Luquillo Experimental Forest. United States Department of Agriculture Forest Service, Southern Forest Experiment Station, New Orleans, LA, USA.

Calder, I.R., Wright, I.R., Murdiyarso, D., 1986. A study of evaporation from tropical rainforest, west Java. J. Hydrol. 89, 13–31.

Chen, F., Schwerdtfeger, P., 1989. Flux-gradient relationships for momentum and heat over a rough natural surface. Quart. J. Roy. Meteorol. Soc. 115, 335–352.

Cuartas, L.A., Tomasella, J., Nobre, A.D., Hodnett, M.G., Waterloo, M.J., Múnera, J.C., 2007. Interception water-partitioning dynamics for a pristine rainforest in Central Amazonia: marked differences between normal and dry years. Agric. Forest Meteorol. 145, 69–83.

Dunin, F.X., O'Loughlin, E.M., Reyenga, W., 1988. Interception loss from eucalypt forest: lysimeter determination of hourly rates for long term evaluation. Hydrol. Process. 2, 315–329.

Dunkerley, D.L., 2009. Evaporation of impact water droplets in interception processes: historical precedence of the hypothesis and a brief literature overview. J. Hydrol. 376, 599–604.

Dykes, A.P., 1997. Rainfall interception from a lowland tropical rainforest in Brunei. J. Hydrol. 200, 260–279.

Finnigan, J.J., Clement, R., Malhi, Y., Leuning, R., Cleugh, H.A., 2003. A re-evaluation of long-term flux measurement techniques. Part I: averaging and coordinate rotation. Boundary-Lay. Meteorol. 107, 1–48.

Foken, T., Wichura, B., 1996. Tools for quality assessment of surface-based flux measurements. Agric. Forest Meteorol. 78, 83–105.

Garratt, J.R., 1992. The Atmospheric Boundary Layer. Cambridge University Press, Cambridge.

Garratt, J.R., Francey, R.J., 1978. Bulk characteristics of heat transfer in the baroclinic atmospheric boundary layer. Boundary-Lay. Meteorol. 15, 399–421.

Gash, J.H.C., 1979. An analytical model of rainfall interception by forests. Quart. J. Roy. Meteorol. Soc. 105, 43–55.

Gash, J.H.C., Morton, A.J., 1978. An application of the Rutter model to the estimation of the interception loss from Thetford forest. J. Hydrol. 38, 49–58.

Gash, J.H.C., Dolman, A.J., 2003. Sonic anemometer (co)sine response and flux measurement. I. The potential for (co)sine error to affect sonic anemometer-based flux measurements. Agric. Forest Meteorol. 119, 195–207.

Gash, J.H.C., Wright, I.R., Lloyd, C.R., 1980. Comparative estimates of interception loss from three coniferous forests in Great Britain. J. Hydrol. 48, 89–105.

Gash, J.H.C., Valente, F., David, J.S., 1999. Estimates and measurements of evaporation from wet, sparse pine forest in Portugal. Agric. Forest Meteorol. 94, 149–158.

García-Martinó, A.R., Warner, G.S., Scatena, F.N., Civco, D.L., 1996. Rainfall, runoff and elevation relationships in the Luquillo Mountains of Puerto Rico. Caribbean J. Sci. 32, 413–424.

Heartsill-Scalley, T., Scatena, F.N., Estrada, C., McDowell, W.H., Lugo, A.E., 2007. Disturbance and long-term patterns of rainfall and throughfall nutrient fluxes in a subtropical wet forest in Puerto Rico. J. Hydrol. 333, 472–485.

Herbst, M., Rosier, P.T.W., McNeil, D.D., Harding, R.J., Gowing, D.J., 2008. Seasonal variability of interception evaporation from the canopy of a mixed deciduous forest. Agric. Forest Meteorol. 148, 1655–1667.

Holwerda, F., 2005. Water and Energy Budgets of Rain Forests Along an Elevational Gradient Under Maritime Tropical Conditions. PhD Thesis, VU University, Amsterdam, The Netherlands. <http://www.falw.vu.nl/nl/onderzoek/earth-sciences/geo-environmental-science-and-hydrology/hydrology-dissertations/index.asp>.

Holwerda, F., Scatena, F.N., Bruijnzeel, L.A., 2006. Throughfall in a Puerto Rican lower montane rain forest: a comparison of sampling strategies. J. Hydrol. 327, 592–602.

Hutjes, R.W.A., Wierda, A., Veen, A.W.L., 1990. Rainfall interception in the Tai Forest, Ivory Coast: application of two simulation models to a humid tropical system. J. Hydrol. 114, 259–275.

Kaimal, J.C., Finnigan, J.J., 1994. Atmospheric Boundary Layer Flows: Their Structure and Measurement. Oxford University Press, New York.

Kamburova, P.L., Ludlam, F.H., 1966. Rainfall evaporation in thunderstorm downdrafts. Quart. J. Roy. Meteorol. Soc. 92, 510–518.

Klaassen, W., Bosveld, F., de Water, E., 1998. Water storage and evaporation as constituents of rainfall interception. J. Hydrol. 212–213, 36–50.

Kumagai, T., Saitoh, T.M., Sato, Y., Takahashi, H., Manfroi, O.J., Morooka, T., Kuraji, K., Suzuki, M., Yasunari, T., Komatsu, H., 2005. Annual water balance and seasonality of evapotranspiration in a Bornean tropical rainforest. Agric. Forest Meteorol. 128, 81–92.

Kume, T., Manfroi, O.J., Kuraji, K., Tanaka, N., Horiuchi, T., Suzuki, M., Kumagai, T., 2008. Estimation of canopy water storage capacity from sap flow measurements in a Bornean tropical rainforest. J. Hydrol. 352, 288–295.

Liu, H., Peters, G., Foken, T., 2001. New equations for sonic temperature variance and buoyancy heat flux with an omnidirectional sonic anemometer. Boundary-Lay. Meteorol. 100, 459–468.

Lloyd, C.R., Marques, A.D., 1988. Spatial variability of throughfall and stemflow measurements in Amazonian rainforest. Agric. Forest Meteorol. 42, 63–73.

Lloyd, C.R., Gash, J.H.C., Shuttleworth, W.J., Marques, A.D., 1988. The measurement and modeling of rainfall interception by Amazonian rain forest. Agric. Forest Meteorol. 43, 277–294.

Manfroi, O.J., Kuraji, K., Suzuki, M., Tanaka, N., Kume, T., Nakagawa, M., Kumagai, T., Nakashizuka, T., 2006. Comparison of conventionally observed interception evaporation in a 100-m^2 subplot with that estimated in a 4-ha area of the same Bornean lowland tropical forest. J. Hydrol. 329, 329–349.

Mizutani, K., Yamanoi, K., Ikeda, T., Watanabe, T., 1997. Applicability of the eddy correlation method to measure sensible heat transfer to forest under rainfall conditions. Agric. Forest Meteorol. 86, 193–203.

Monteith, J.L., 1965. Evaporation and the environment. Symp. Soc. Exp. Biol. 19, 245–269.

Monteith, J.L., Unsworth, M.H., 2008. Principles of Environmental Sciences. Elsevier, Amsterdam.

Murakami, S., 2006. A proposal for a new forest canopy interception mechanism: splash droplet evaporation. J. Hydrol. 319, 72–82.

Murakami, S., 2007. Application of three canopy interception models to a young stand of Japanese cypress and interpretation in terms of interception mechanism. J. Hydrol. 342, 305–319.

Muzylo, A., Llorens, P., Valente, F., Keizer, J.J., Domingo, F., Gash, J.H.C., 2009. A review of rainfall interception modeling. J. Hydrol. 370, 191–206.
Nakai, T., van der Molen, M.K., Gash, J.H.C., Kodama, Y., 2006. Correction of sonic anemometer angle of attack errors. Agric. Forest Meteorol. 136, 19–30.
Odum, H.T., Abbot, W., Selander, R.K., Golley, F.B., Wilson, R.F., 1970. Estimates of chlorophyll and biomass of the Tabonuco forest of Puerto Rico. In: Odum, H.T., Pigeon, R.F. (Eds.), A Tropical Rain Forest. United States Atomic Energy Commission, Washington, DC, USA.
Panofsky, H.A., Tennekes, H., Lenschow, D.H., Wyngaard, J.C., 1977. The characteristics of turbulent velocity components in the surface layer under convective conditions. Boundary-Lay. Meteorol. 11, 355–361.
Paulson, C.A., 1970. The mathematical representation of wind speed and temperature profiles in the unstable atmospheric surface layer. J. Appl. Meteorol. 9, 857–861.
Raupach, M.R., Finnigan, J.J., 1997. The influence of topography on meteorological variables and surface–atmosphere interactions. J. Hydrol. 190, 182–213.
Roberts, J.M., Gash, J.H.C., Tani, M., Bruijnzeel, L.A., 2005. Controls on evaporation in lowland tropical rainforest. In: Bonell, M., Bruijnzeel, L.A. (Eds.), Forests, Water and People in the Humid Tropics. Cambridge University Press, Cambridge, UK, pp. 287–313.
Rutter, A.J., Kershaw, K.A., Robins, P.C., Morton, A.J., 1971. A predictive model of rainfall interception in forests, 1. Derivation of the model from observations in a plantation of Corsican pine. Agric. Meteorol. 9, 367–384.
Rutter, A.J., Morton, A.J., Robins, P.C., 1975. A predictive model of rainfall interception in forests. II. Generalization of the model and comparison with observations in some coniferous and hardwood stands. J. Appl. Ecol. 12, 367–380.
Scatena, F.N., 1990. Watershed scale rainfall interception on two forested watersheds in the Luquillo Mountains of Puerto Rico. J. Hydrol. 113, 89–102.
Scatena, F.N., Lugo, A.E., 1995. Geomorphology, disturbance, and the soil and vegetation of two subtropical wet steepland watersheds of Puerto Rico. Geomorphology 13, 199–213.
Scatena, F.N., Moya, S., Estrada, C., Chinea, J.D., 1996. The first five years in the reorganization of aboveground biomass and nutrient use following hurricane Hugo in the Bisley experimental watersheds, Luquillo Experimental Forest, Puerto Rico. Biotropica 28, 424–440.
Schellekens, J., Scatena, F.N., Bruijnzeel, L.A., Wickel, A.J., 1999. Modelling rainfall interception by a lowland tropical rain forest in northeastern Puerto Rico. J. Hydrol. 225, 168–184.
Schellekens, J., Bruijnzeel, L.A., Scatena, F.N., Bink, N.J., Holwerda, F., 2000. Evaporation from a tropical rain forest, Luquillo Experimental Forest, eastern Puerto Rico. Water Resour. Res. 36, 2183–2196.
Schuepp, P.H., Leclerc, M.Y., Macpherson, J.I., Desjardins, R.L., 1990. Footprint prediction of scalar fluxes from analytical solutions of the diffusion equation. Boundary-Lay. Meteorol. 50, 353–373.
Shuttleworth, W.J., 1988. Evaporation from Amazonian rainforest. Proc. Roy. Soc. London: Ser. B, Biol. Sci. 233, 321–346.
Shuttleworth, W.J., 1989. Micrometeorology of temperate and tropical forest. Philos. Trans. Roy. Soc. London: Ser. B, Biol. Sci. 324, 299–334.
Shuttleworth, W.J., Calder, I.R., 1979. Has the Priestley–Taylor equation any relevance to forest evaporation? J. Appl. Meteorol. 18, 639–646.
Simpson, I.J., Thurtell, G.W., Nuemann, H.H., den Hartog, G., Edwards, G.C., 1998. The validity of similarity theory in the roughness sublayer above forests. Boundary-Lay. Meteorol. 87, 69–99.
Sozzi, R., Favaron, M., 1996. Sonic anemometry and thermometry: theoretical basis and data-processing software. Environ. Softw. 11, 259–270.
Stewart, J.B., 1977. Evaporation from the wet canopy of a pine forest. Water Resour. Res. 13, 915–921.
Stull, R.B., 1988. An Introduction to Boundary Layer Meteorology. Kluwer Academic Press, Dordrecht, The Netherlands.
Thom, A.S., 1972. Momentum, mass and heat exchange of vegetation. Quart. J. Roy. Meteorol. Soc. 98, 124–134.
Thom, A.S., 1975. Momentum, mass and heat exchange of plant communities. In: Monteith, J.L. (Ed.), Vegetation and the Atmosphere, 1. Principles. Academic Press, London, pp. 57–109.
Thom, A.S., Stewart, J.B., Oliver, H.R., Gash, J.H.C., 1975. Comparison of aerodynamic and energy budget estimates of fluxes over a pine forest. Quart. J. Roy. Meteorol. Soc. 101, 93–105.
Thomas, C., Foken, T., 2002. Re-evaluation of integral turbulence characteristics and their parameterisations. In: 15th Symposium on Boundary Layers and Turbulence. American Meteorological Society, Wageningen, The Netherlands, pp. 129–132.
US Geological Survey, 2010. National Water Information System Data Available on the World Wide Web (Water Data for the Nation). <http://waterdata.usgs.gov/pr/nwis/uv/?site_no=50065549&agency_cd=USGS> (accessed 29.12.10).
Van der Molen, M.K., 2002. Meteorological Impacts of Land Use Change in the Maritime Tropics. PhD Thesis, VU University, Amsterdam, The Netherlands. <http://www.falw.vu.nl/nl/onderzoek/earth-sciences/geo-environmental-science-and-hydrology/hydrology-dissertations/index.asp>.
Van der Molen, M.K., Gash, J.H.C., Elbers, J.A., 2004. Sonic anemometer (co)sine response and flux measurement II. The effect of introducing an angle of attack dependent calibration. Agric. Forest Meteorol. 122, 95–109.
Van der Tol, C., Gash, J.H.C., Grant, S.J., McNeil, D.D., Robinson, M., 2003. Average wet canopy evaporation for a Sitka spruce forest derived using the eddy correlation-energy balance technique. J. Hydrol. 276, 12–19.
Van Gorsel, E., Christen, A., Feigenwinter, C., Parlow, E., Vogt, R., 2003. Daytime turbulence statistics above a steep forested slope. Boundary-Lay. Meteorol. 109, 311–329.
Vernimmen, R.R.E., Bruijnzeel, L.A., Romdoni, A., Proctor, J., 2007. Rainfall interception in three contrasting lowland rain forest types in Central Kalimantan, Indonesia. J. Hydrol. 340, 217–232.
Wallace, J., McJannet, D., 2008. Modelling interception in coastal and montane rainforests in northern Queensland, Australia. J. Hydrol. 348, 480–495.
Watanabe, T., Mizutani, K., 1996. Model study on micrometeorological aspects of rainfall interception over an evergreen broad-leaved forest. Agric. Forest Meteorol. 80, 195–214.
Waterloo, M.J., 1994. Water and Nutrient Dynamics of *Pinus caribaea* Plantation Forests on Former Grassland Soils in Viti levu, Fiji. PhD Thesis, VU University, Amsterdam, The Netherlands. <http://www.falw.vu.nl/nl/onderzoek/earth-sciences/geo-environmental-science-and-hydrology/hydrology-dissertations/index.asp>.
Waterloo, M.J., Bruijnzeel, L.A., Vugts, H.F., 1999. Evaporation from *Pinus caribaea* plantations on former grassland soils under maritime tropical conditions. Water Resour. Res. 35, 2133–2144.
Webb, E.K., 1970. Profile relationships: the log-linear range, and extension to strong stability. Quart. J. Roy. Meteorol. Soc. 96, 67–90.
Weber, R.O., 1999. Remarks on the definition and estimation of friction velocity. Boundary-Lay. Meteorol. 93, 197–209.
Ziegler, A.D., Giambelluca, T.W., Nullet, M.A., Sutherland, R.A., Tantasarin, C., Vogler, J.B., Negishi, J.N., 2009. Throughfall in an evergreen-dominated forest stand in northern Thailand: comparison of mobile and stationary methods. Agric. Forest Meteorol. 149, 373–384.
Zimmermann, B., Zimmermann, A., Lark, R.M., Elsenbeer, H., 2010. Sampling procedures for throughfall monitoring: a simulation study. Water Resour. Res. 46, W01503, 10.1029/2009WR00776.